

Reactive Power Compensation for an Induction Generator Using Series STATCOM for AC Microgrids

A project report submitted
in partial fulfillment for the award of the degree of

Bachelor of Technology

in

Electronics and Communication Engineering
(with specialization in Avionics)

by

Chunduri Sai Abhishek



Department of Avionics
Indian Institute of Space Science and Technology
Thiruvananthapuram, India

May 2022

Certificate

This is to certify that the project report titled ***Reactive Power Compensation for an Induction Generator Using Series STATCOM for AC Microgrids*** submitted by **Chunduri Sai Abhishek**, to the Indian Institute of Space Science and Technology, Thiruvananthapuram, in partial fulfillment for the award of the degree **Bachelor of Technology in Electronics and Communication Engineering (with specialization in Avionics)**, is a bonafide record of the original work carried out by him under our supervision. The contents of this report, in full or in parts, have not been submitted to any other Institute or University for the award of any degree or diploma.

Dr. R. Sudharshan Kaarthik

Dr. Rajeevan P.P.

Associate Professor

Department of Avionics

Dr. Deepak Mishra

Professor & Head

Department of Avionics

Place: Thiruvananthapuram

Date: May 2022

Declaration

I declare that this project report titled ***Reactive Power Compensation for an Induction Generator Using Series STATCOM for AC Microgrids*** submitted in partial fulfillment for the award of the degree **Bachelor of Technology in Electronics and Communication Engineering (with specialization in Avionics)** is a record of original work carried out by me under the supervision of **Dr. R. Sudharshan Kaarthik** and **Dr. Rajeevan P.P.**, and has not formed the basis for the award of any degree, diploma, associateship, fellowship, or other titles in this or any other Institution or University of higher learning. In keeping with the ethical practice in reporting scientific information, due acknowledgments have been made wherever the findings of others have been cited.

Place: Thiruvananthapuram

Chunduri Sai Abhishek

Date: May 2022

(SC18B114)

Acknowledgements

I would like to thank my guide, Dr.R. Sudharshan Kaarthik, Associate Professor, Department of Avionics, IIST, for giving me a chance to work on this topic as a part of my final year project . I am very grateful for the tremendous support and guidance he has provided me at every stage of my work. We came across several errors and debugging issues during the project in the simulation phase. He was patient enough to clear all my doubts, point out the mistakes, and help me correct them, which eventually led to successful results.

I would also like to express my gratitude to thank Dr. Rajeevan P.P., Associate Professor, Department of Avionics, IIST, for sharing his expertise in power electronics converters and AC drives . He always guided me on what next and what new extensions could be done in the project and helped me set up the hardware. He directed the whole experimental setup and procedures step-by-step, enabling me to understand practical system implementations better.

Without the support of M.Tech and Ph.D. seniors in the "Power Electronics Research Laboratory (L004)", my project would just have been an idea limited to simulations. The constant guidance and support from Mohit Kumar, Aishwarya, Vidya V, Hari, Balwant K, Deeksha, and Prasoon enabled me to understand and develop the DSP C codes and the hardware systems. From debugging the codes to running such massive systems, they were always there to help me out.

Without the support of my family, parents, and my brother, it would not have been possible to finish the project. I am thankful to every faculty of IIST for providing me little gradient directions to improvise myself . It has been a pride and pleasure to learn under them. I hope to make them proud one day. Finally, I would like to acknowledge my friends Akshaj Jangiti, K Raghavendra, U Dhana Ganesh, Ch Bhargav, Meghana Imandi, Jishil Jinaraj, J Sai Rohith, Praneeth Varma, and Hepsiba for their suggestions, companionship, and for making interactions in IIST enjoyable. I also thank my entire batch and the IIST family for the glorious four years. Their friendship was a blessing for me, not only during the project but throughout my four years of B.Tech life.

Chunduri Sai Abhishek

Abstract

Induction generators (IGs) are commonly used in power generation systems such as wind generators and hydro turbine systems. IGs are used primarily to meet the auxiliary power requirements in electric vehicles (EVs), more electric aircrafts (MEAs), and urban windmills. The shafts of the induction machine are coupled to the main engine shaft, and IG draws the required power from the main engine.

The conventional IG systems are based on a shunt compensating architecture for providing the necessary reactive power to the IG. Such an architecture would require interfacing inductors between the grid and the IG, which increases the size and weight of the system. This report presents a series compensation-based architecture for grid and grid plus load connected IG systems. The necessary reactive power is fed by a capacitive fed voltage source inverter (VSI) in a series compensation scheme. An IG with an open-end stator winding configuration is used for this purpose. The VSI meets the reactive power requirements of loads and IG, and the IG meets the active power requirements of loads and grid. The requirements like constant DC link voltage and maintenance of unity power factor (UPF) near the grid are met with the help of a vector-based control scheme approach that uses two PI controllers. The grid plus load connected system is similar to the architecture in present-day AC microgrids, and hence the applications of such a system are presented.

The presented systems are validated for linear balanced (R and RL) loads, linear unbalanced (R and RL) loads and non-linear (DBR) loads using PLECS v4.5.6 software, and the simulation results are included. The experimental setups of the systems and the results are also included.

Contents

List of Figures	xiii
List of Tables	xvii
Nomenclature	xix
1 Introduction	1
1.1 Induction Machines	1
1.2 Literature Review of Existing IG Systems	2
1.3 IG with open-end stator windings	4
1.4 Objectives of the Project	5
1.5 Outline of the Thesis	5
2 Induction Generator and Series Reactive Power Compensation Schemes	7
2.1 Introduction	7
2.2 Basic Terminology and Notations used	7
2.2.1 Torque-Slip Characteristics of an IM	8
2.3 Reactive Power Compensation for Grid-Connected IG system using series STATCOM	9
2.3.1 Power Flow in the System	10
2.3.2 Operation and Working of the Circuit	10
2.3.3 Control Architecture used for Grid Connected IG System	12
2.4 Reactive Power Compensation for Grid and Load Connected IG system using series STATCOM	15
2.4.1 Power Flow in the System	16
2.4.2 Control Architecture used for Grid and Load Connected IG System	17
2.5 Application to AC Microgrids	20

2.5.1	Power Flow in different modes of operation	21
2.5.1.1	Normal Mode of Operation	21
2.5.1.2	Generator Mode of Operation	21
2.5.1.3	Island Mode of Operation	21
2.6	Conclusion	22
3	Simulation Results	23
3.1	Introduction	23
3.2	Parameters of the Induction Machine	23
3.3	Simulation Results for Series Reactive Power Compensation of Grid-Connected IG	24
3.3.1	Setting up the IM in Generator Mode	24
3.3.2	Phase Reversal in Stator Currents	25
3.3.3	DC Link Voltage	26
3.3.4	Flow of Active and Reactive Power in the system	27
3.4	Simulation Results for Series Reactive Power Compensation of Grid and Load Connected IG	29
3.4.1	DC Link Voltage	29
3.4.2	Flow of Active and Reactive Power	30
3.4.2.1	Linear Resistive (R) Loads	30
3.4.2.2	Linear RL Loads	32
3.4.2.3	Non-Linear DBR Load	35
3.5	Conclusion	37
4	Hardware Modules and Experimental Results	38
4.1	Introduction	38
4.2	Hardware Modules	38
4.3	Experimental Results	39
4.3.1	Implementation of Sine-Triangle PWM on DSP Module	39
4.3.2	Implementation of Reference Frame Transformations on DSP Module	41
4.3.2.1	Clarke's Transformation	43
4.3.2.2	Inverse Clarke's Transformation	44
4.3.2.3	Theta (θ) Estimation using 3- ϕ PLL	45
4.3.2.4	Park's Transformation	45
4.3.2.5	Inverse Park's Transformation	46
4.3.3	Setting up the Induction Machine in Generator Mode	47

4.3.4	Reactive Power Compensation using VSI	50
4.4	Conclusions	54
5	Conclusions and Future Works	55
5.1	Results and Discussion	55
5.2	Future Works	56
Bibliography		56
Appendices		61
A	Appendix A	61
A.1	Hardware Modules	61
A.1.1	3- ϕ Auto-transformer	61
A.1.2	Voltage Sensor Board	62
A.1.3	Level Shifter Board	62
A.1.4	TI TMS320F28069M DSP Board	63
A.1.4.1	Specifications of the TMS320F28069M DSP Module . .	64
A.1.4.2	Modules of DSP	64
A.1.4.3	Enhanced Pulse Width Modulation (ePWM)	64
A.1.4.4	Enhanced Quadrature Encoder Pulse (eQEP)	65
A.1.4.5	Analog to Digital Converter (ADC)	65
A.1.5	3- ϕ Inverter	65
A.1.6	Hall Effect Current Sensors	66
A.1.7	3- ϕ Induction Generator with open-end stator windings	67

List of Figures

1.1	Different modes of operation of IG systems.	3
1.2	Conventional schemes used in grid-connected systems.	3
2.1	Torque-Slip characteristics of a 3- ϕ IM.	8
2.2	Series compensated grid-connected system.	9
2.3	Equivalent circuit of the grid-connected IG system.	10
2.4	Phasor diagrams and vectors involved in the control scheme.	12
2.5	Overall control architecture used for series compensation of grid connected IG system.	14
2.6	Series compensated grid and load connected system.	15
2.7	Various kind of loads considered for analysis.	16
2.8	Phasor diagram of grid and load connected IG system.	18
2.9	Overall control architecture used for series compensation of grid and load connected IG system.	19
2.10	IG based AC microgrid architecture.	20
3.1	Load torque and speed characteristics of the system.	24
3.2	Stator phase currents of the grid-connected IG system.	25
3.3	DC link voltage across the capacitor of VSI.	26
3.4	Plot of inverter leg voltage and machine current.	27
3.5	Plot of grid phase voltage and grid phase currents.	28
3.6	DC link voltage across the capacitor of VSI for various loads.	29
3.7	Simulation Results for balanced R Load.	31
3.8	Simulation Results for unbalanced R Load.	31
3.9	Inverter pole voltage and machine currents for resistive load.	32
3.10	Simulation Results for balanced RL Load.	33
3.11	Simulation Results for unbalanced RL Load.	34

3.12	Inverter pole voltage and machine currents for an RL load.	34
3.13	Simulation Results for a non-linear DBR Load.	35
3.14	UPF being maintained in case of non-linear DBR load	36
3.15	Inverter pole voltage and machine currents for a non-linear load.	36
4.1	Switching pulses for top and bottom switches.	40
4.2	CCS code snippet for SPWM implementation.	40
4.3	Switching pulses and corresponding modulating sine wave.	41
4.4	Output of voltage sensor and level shifter module.	42
4.5	CCS code snippet for voltage sensing using ADC.	42
4.6	CCS code snippet for reference frame transformations.	43
4.7	V_{abc} phase voltages sensed and processed by DSP.	43
4.8	$V_{\alpha\beta}$ components of the voltage obtained from DSP.	44
4.9	V_{abc} components back estimated from $V_{\alpha\beta}$	44
4.10	θ estimated using the 3- ϕ PLL.	45
4.11	V_{dq} components estimated from simulation in PLECS.	46
4.12	V_{dq} components obtained from DSP Module and plotted via MATLAB. . .	46
4.13	V_{dq} components obtained from DSP.	47
4.14	V_{abc} components back estimated from V_{dq}	47
4.15	Winding configuration used to configure the machine as a 3- ϕ IM.	48
4.16	Circuit diagram to setup the IM in generation mode.	49
4.17	Stator phase currents in motoring and generator mode.	50
4.18	Transition from motoring to generating mode.	50
4.19	Circuit diagram of experimental setup of IG with series compensation. . .	51
4.20	Experimental Setup of the IG with reactive power compensation using VSI. .	52
4.21	Output of 90° phase shift filter implemented on DSP.	52
4.22	Waveforms during transition from motoring to generating mode.	53
4.23	Waveforms in motoring and generating mode.	53
4.24	Machine current and inverter voltage in motoring and generating mode. .	54
A.1	3- ϕ Auto-transformer in Laboratory.	61
A.2	3-channel Voltage Sensor Module.	62
A.3	Level Shifter Module.	63
A.4	TMS320F28069M DSP Module.	64
A.5	3- ϕ Inverter Module with DBR and Hall-Effect Current/Voltage Sensors. .	66
A.6	Hall-Effect based Current Sensors.	66

A.7 3- ϕ Induction Machine with DC Motor.	67
--	----

List of Tables

2.1	Notations and Parameters used	11
2.2	Difference between Grid Connected, Grid and Load Connected IG Systems	20
2.3	Different Modes of Operation of IG based Microgrid Architecture	21
3.1	Parameters of IG used during simulation.	24
A.1	Specifications of Induction Machine and DC Motor	67

Nomenclature

AC	Alternating Current
ADC	Analog to Digital Converter
CCS	Code Composer Studio
CVVF	Constant Voltage Variable Frequency
DAC	Digital to Analog Converter
DBR	Diode Bridge Rectifier
DC	Direct Current
DSP	Digital Signal Processor
ePWM	Enhanced Pulse Width Modulation
eQEP	Enhanced Quadrature Encoder Pulse
EV	Electric Vehicle
GPIO	General Purpose Input/Output
IG	Induction Generator
IGBT	Insulated Gate Bipolar Transistor
IM	Induction Machine
MEA	More Electric Aircraft
PCC	Point of Common Coupling
PI	Proportional Integral
PM	Permanent Magnet
PWM	Pulse Width Modulation
RPM	Revolutions Per Minute
SPWM	Sinusoidal Pulse Width Modulation
TI	Texas Instruments

Chapter 1

Introduction

1.1 Induction Machines

In today's world, induction machines (IM) are widely used in various applications. IMs play an essential role in some areas, including wind-power generation systems, electric vehicles (EVs), more electric aircrafts (MEAs), etc. Induction machines come with the merits of having simple and rugged construction, low cost, maintenance-free operation, and good operating characteristics [1],[2], [3], [4]. The main principle behind the working of an IM is Faraday's Law of Electromagnetic Induction.

An IM has two main parts: (a) stator (stationary part) and (b) rotor (rotating part). They are also called asynchronous machines because they run at speed not equal to the speed of the rotating magnetic field in the stator (synchronous speed). Induction machines can be run in two modes: (a) IM as a motor and (b) IM as a generator .

The induction machine acts as an induction generator (IG) when its rotor is driven at a speed higher than the stator's rotating magnetic field (synchronous speed). This will result in a negative slip, the machine torque gets reversed, and the machine starts generating. "For an induction generator to deliver active power, it needs reactive power to set up the rotating magnetic field for its operation" [4], [5], [6], [7]. Hence the necessary and sufficient conditions for an induction machine to run as an induction generator are

- Necessary excitation must be provided to the machine.
- Rotor speed (ω_r) must be greater than the synchronous speed (ω_s).

When the rotor frequency exceeds the stator frequency, an adequate amount of excitation ensures successful voltage build-up of the machine.

1.2 Literature Review of Existing IG Systems

Two modes of an induction generator are as follows - (a) Standalone (off-grid) operation and (b) Grid-connected operation. In off-grid-based architectures, the required reactive power is provided with the help of capacitor banks, which are connected in a shunt manner to the IG windings. A fixed capacitor alone cannot ensure adequate reactive power under all speeds or loading conditions. Opting for a switched capacitor system can also control the terminal voltage in discrete steps. These methods cannot ensure adequate reactive power under varying input or output conditions. To avoid the issues mentioned above, nowadays, static VAR compensators, also referred to as STATCOMs, are being used for exciting standalone IG systems [1], [8].

In grid-connected-based architectures, all of the needed reactive power to set up the magnetic field of the IG is drawn from the grid. In the generation mode, the IG will supply active power to the grid but will be consuming the required reactive from the grid [1], [6] . This adds a burden to the grid, and also UPF is not maintained in this case. Hence, nowadays, the grid-connected systems are employed with the help of various other reactive power compensation schemes [8] or some compensating devices are explicitly provided to provide the required reactive power separately. The existing architectures for both off-grid and grid-connected systems are summarized in Fig. 1.1.

Frequency insensitive loads are those loads that require a constant voltage across their terminals irrespective of the frequency of the voltage. They are also referred to as constant voltage variable frequency loads (CVVF). In applications like MEAs and EVs, there are

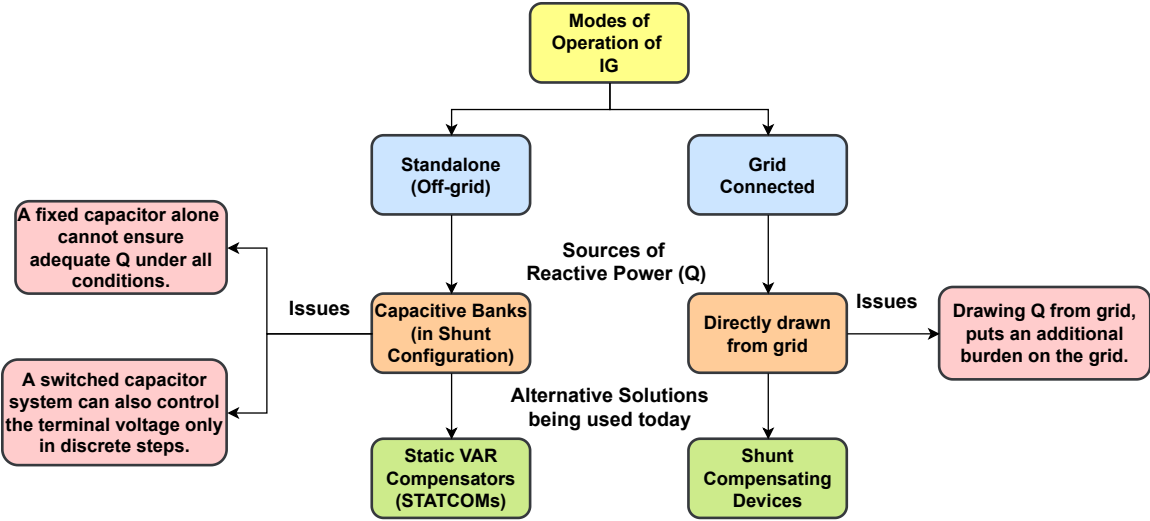


Figure 1.1: Different modes of operation of IG systems.

various frequency insensitive loads like heating, air-conditioning, lighting, and wing deicing systems.

In Fig. 1.2, a conventional shunt compensating scheme for an IG with CVVF AC loads is shown. The STATCOM provides the required reactive power (Q) for the excitation of the machine and loads, and the IG supplies the active power (P) required by the loads. However, as seen in Fig. 1.2, the scheme requires current filters (interfacing inductors) between the loads and the VSI. This adds additional weight, size, and losses to the system.

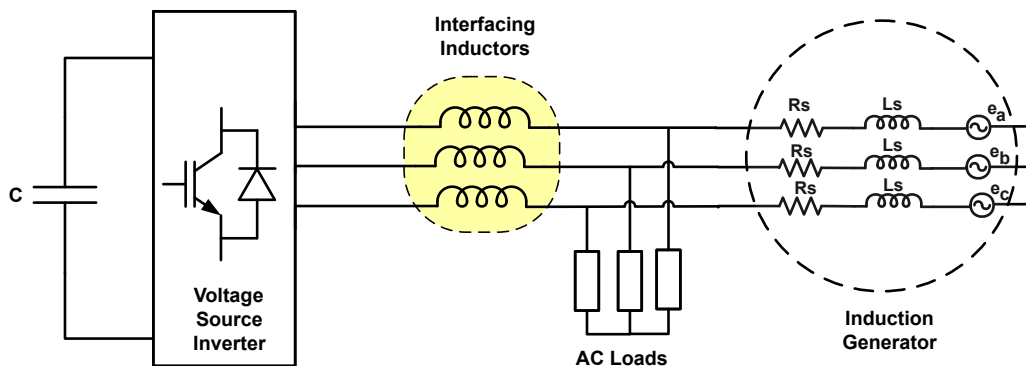


Figure 1.2: Conventional shunt compensating device scheme used in grid connected systems.

In most research, permanent generators (PM) are used for frequency insensitive loads. However, using IG in power generation for auxiliary loads is more beneficial than using

other machines like PM generators. This is because the terminal voltage of the PM generator varies with the speed of the machine. AC voltage generated is first converted to DC and then inverted back to AC of the required voltage level. This involves a two-stage AC-DC-AC conversion which adds additional hardware to the system. This two-stage converter can be avoided by replacing PM generators with induction generators. Also, the magnetic cores used in PM generators tend to slowly lose their magnetic nature over time due to the vast temperature fluctuations that they regularly face when used in electric aircraft. The induction generator does not have such constraints based on the operating temperature and magnetic properties.

1.3 IG with open-end stator windings

The shunt-based architectures and STATCOMs for reactive power compensation have been widely used in IG systems for decades. However, the idea of series compensation is something new and slowly developing. The idea of series compensation would require an IG in which both ends are accessible for the series connections. Hence, an open-end stator winding-based induction machine is used for this purpose [9], [10]. An open-end stator winding IM is simply a standard squirrel cage-based IG. Both the ends of stator windings are terminated externally instead of the usual way of connecting them in star or delta. An IG system using open-end windings with a battery-powered series compensator is discussed in [11].

Similarly, a permanent magnet synchronous generator-based system with series reactive power compensation is discussed in [12]. Standalone IG systems with series compensation schemes and frequency insensitive AC loads used in more electric aircrafts (MEA) are presented in [13]. Various control architectures for series compensation of off-grid IG systems with open end stator windings and frequency insensitive loads are discussed in [14].

There is a fundamental difference between the control architectures used for off-grid and grid-connected systems. The grid voltage and frequency are constant in grid-connected systems and cannot vary based on generator conditions. The IG supplies power to the grid, and grid voltage is constant. The grid decides the frequency at which the IG operates. However, in the case of off-grid systems, the generator operating point (voltage and frequency) is determined by the load.

1.4 Objectives of the Project

Applications like electric vehicles (EVs), more electric aircraft (MEA), etc., consist of auxiliary electrical loads that are frequency insensitive, such as heating loads, wing-deicing systems, lighting, and low-voltage DC housekeeping supplies. This forms the motivation for the objectives of our project, which are as follows:

- To review the existing series reactive power compensation technique for grid-connected IG systems and load connected IG systems (stand-alone).
- To familiarize with various hardware modules like VSI, induction motor/generator, DC motor, DBRs, current/voltage sensors, and software modules like TI DSP board and CCS platform and implement control schemes using them.
- To develop a control architecture for series reactive power compensation for grid plus load connected IG system and extend this idea to microgrid applications.
- To simulate and experimentally validate the above-developed scheme for grid plus load connected IG system.

1.5 Outline of the Thesis

Chapter 1 gives an overview of induction machines and the necessary conditions to run them as generators. The literature review of the existing IG systems is also provided in this

chapter. Chapter 2 focuses on the two kinds of IG systems, i.e., grid-connected and grid plus load connected. The principle of operation and control schemes for both systems are discussed in this chapter. The extension of the grid plus load connected system is microgrids is also discussed in this chapter. Chapter 3 focuses on the simulation results of the grid connected system and grid plus load connected system for various loads. In Chapter 4, the experimental results taken during the setup of systems, along with the hardware connection setup diagrams, are mentioned. The report ends with Chapter 5, in which conclusions and future works of this project are mentioned.

Chapter 2

Induction Generator and Series Reactive Power Compensation Schemes

2.1 Introduction

This chapter discusses the basic terminologies linked with induction machines and induction generators. The grid-connected IG system with series reactive power compensation is discussed in detail, along with the circuit diagram and control architecture. The extension to the grid-connected system, i.e., grid and load connected system, is also presented in this chapter. The differences between the systems, phasor diagrams, and control architectures are presented. The chapter provides an application of grid and load-connected system topology to AC microgrids.

2.2 Basic Terminology and Notations used

In an IM, the rotating magnetic field produced by the stator causes the rotor to run behind it at less than synchronous speed. The speed of the rotating magnetic field is often referred to as synchronous speed (ω_s). The speed of the rotor is called rotor speed (ω_r). The difference between the synchronous speed and the speed of the rotor is known as slip speed (ω_{slip}).

The following equations define slip, slip speed, and synchronous speed (N_s expressed in revolutions per minute), respectively. Here, f_s is the supply frequency, and p is the number of poles in the motor.

$$\omega_{slip} = \omega_s - \omega_r \quad (2.1)$$

$$Slip = s = \frac{\omega_{slip}}{\omega_s} \quad (2.2)$$

$$Synchronous Speed = N_s = \frac{120f_s}{p} \text{ rpm} \quad (2.3)$$

If the rotor is made to rotate at speed greater than the synchronous speed, the slip becomes negative. Under this condition, the IM will operate as an induction generator and will start generating power. When the generator action begins, a phase reversal (180° phase shift) in stator current and stator terminal voltage can be observed.

2.2.1 Torque-Slip Characteristics of an IM

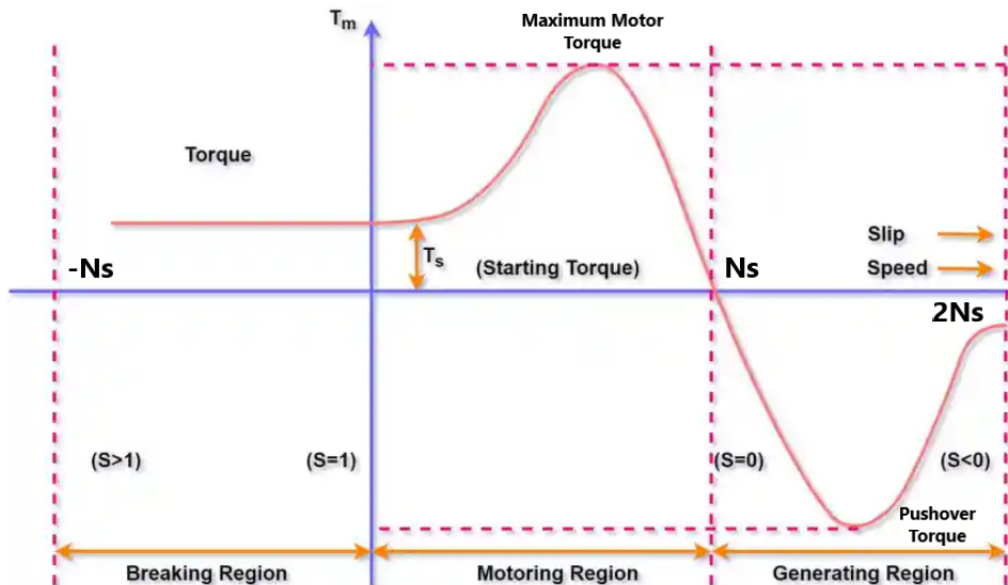


Figure 2.1: Torque-Slip characteristics of a 3- ϕ IM.

The torque-slip curve of an IM gives us the information about the variation of torque with the slip, and it is as shown in Fig. 2.1 [15]. Torque is proportional to slip at low slips, near the synchronous frequency. The maximum torque beyond which the machine stalls at low slip values is called the breakdown torque or the pushover torque. In motoring operation slip is positive ($s > 0$), and in generating mode of operation slip is negative ($s < 0$).

2.3 Reactive Power Compensation for Grid-Connected IG system using series STATCOM

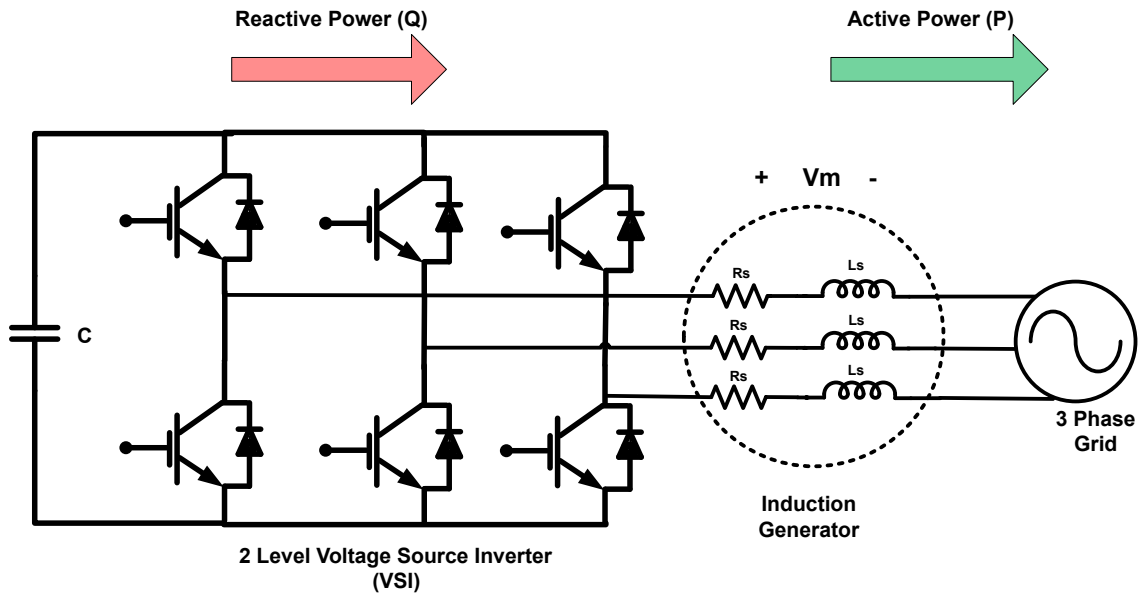


Figure 2.2: Circuit diagram for the series compensation of grid-connected IG system.

First, an induction generator with open-end stator windings is considered. One side of the windings is connected to the capacitor fed VSI, and the windings on the other side are connected to the grid [16]. As seen in Fig. 2.2, the scheme has no interfacing inductors (current filters) involved between the VSI and IG. Hence, the overall system's weight, size, and losses can be reduced. In the series compensation scheme, the machine windings act as interfacing inductors between the grid and VSI. The current filters in shunt schemes provide the reference 'reactive current', but in the series compensation schemes, the required

reference ‘reactive voltage’ is provided by the VSI.

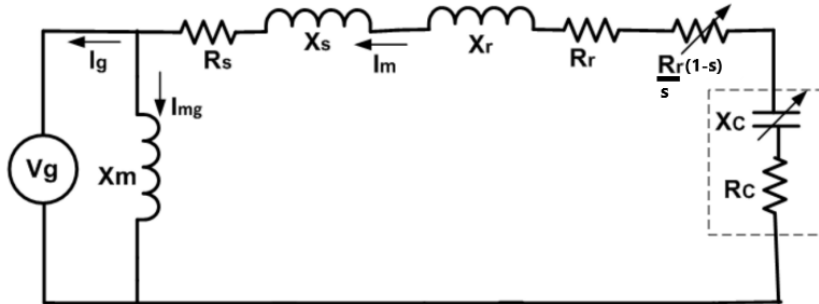


Figure 2.3: Equivalent circuit of the grid-connected IG system with series compensation.

2.3.1 Power Flow in the System

The VSI provides all the reactive power needed for the excitation of the VSI . Since this is a grid-connected system, the grid frequency and the fundamental frequency of VSI output are the same. Since all the components (VSI, IG, and grid) are connected in a series fashion, the same current will flow through them. This current is referred to as generator current (I_m). The IG should supply active power to the grid without consuming any reactive power . A vector-based control loop ensures unity power factor (UPF) and maintains a stable DC link voltage. It also has to ensure that the phase difference between the fundamental component of VSI (V_{in}) and generator current (I_m) is 90° . In practical cases, the voltage across the capacitor will reduce due to losses in the capacitor and inverter. So, in such cases, a small amount of active power is also drawn by the VSI to maintain the constant DC link voltage.

2.3.2 Operation and Working of the Circuit

The equivalent circuit of the system is shown in Fig. 2.3. Under the steady-state condition, from KVL, KCL, and power balance, the following equations hold:

Table 2.1: Notations and Parameters used

Notation	Description
V_g	Grid Voltage
I_g	Grid Current
I_m	Generator Current
I_{mg}	Magnetizing Current
V_{in}	Fundamental Component of VSI
s	Slip
R_s	Stator Resistance
X_s	Stator Leakage Reactance
R_r	Rotor Resistance
X_r	Rotor Leakage Reactance
R_c	Losses in Capacitor and Inverter
X_c	Variable Capacitor (Model of VSI)
X_m	Magnetizing Reactance

$$V_g \cdot I_g + I_m^2 (R_s + R_r + R_c) = I_m^2 R_r \left(\frac{1}{s} - 1 \right) \quad (2.4)$$

$$I_{mg}^2 X_m + I_m^2 (X_s + X_r) = I_m^2 X_c \quad (2.5)$$

The term $I_m^2 R_r \left(\frac{1}{s} - 1 \right)$ represents the active power that the IG produces. With the help of a control scheme, UPF is ensured. So, the term $V_g \cdot I_g$ denotes the active power being supplied to the grid by the IG. The term $I_m^2 X_c$ denotes the amount of reactive power the VSI supplies. The VSI is modeled as a variable capacitance with a capacitance value of X_c . VSI will supply all the reactive power needed for the excitation of the IG for all values of generator current. Only a small part of the generator current will be getting lost as the magnetizing current component I_{mag} . So, the machine current at full load (I_m) and generator current (I_g) at full load will be approximately the same.

$$|V_{in}| = \sqrt{|V_m|^2 - |V_g|^2} \quad (2.6)$$

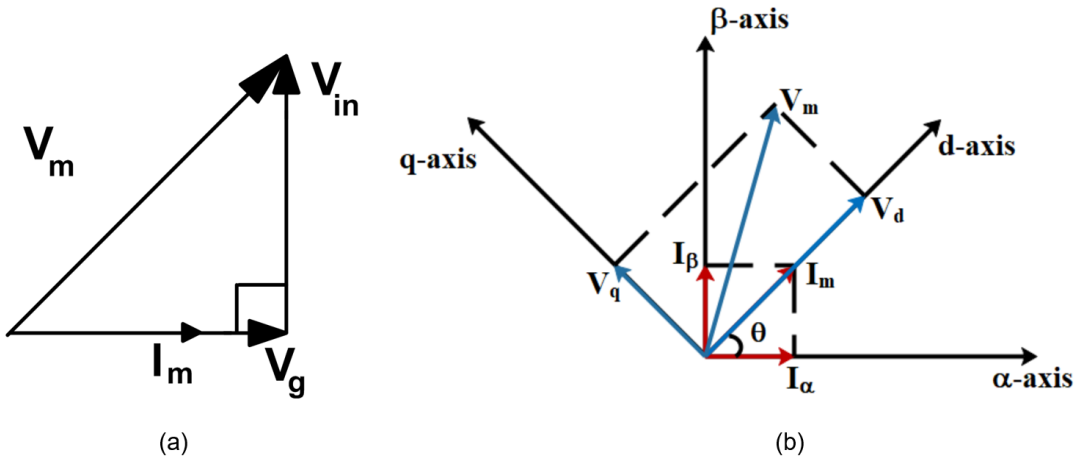


Figure 2.4: (a) Phasor relationship between the I_m , V_{in} , V_m , and V_g (b) Voltage and current phasors used in the vector-control scheme (represented in a rotating dq reference frame).

The magnitude and angle of the inverter voltage phasor (VSI output voltage) are constrained as per the phasor diagram Fig. 2.4, and Eq-2.6. Ideally, the VSI should only provide the needed reactive power to the IG for its excitation and should not consume any active power. Hence, the inverter voltage (V_{in}) and generator current (I_m) must be in quadrature with each other, as shown in Fig. 2.4.

2.3.3 Control Architecture used for Grid Connected IG System

The control scheme employed must ensure the following three things :

- Maintain a 90° phase shift between V_{in} and $I_{machine}$. This ensures that active power is not supplied from the VSI.
- Maintain Unity Power Factor (UPF) at grid end, i.e., V_{grid} and I_{grid} must be in phase. This ensures that only active power is transferred between IG and the grid, and no reactive power flow happens between them.
- To maintain a constant voltage across the capacitor of the VSI under all operating conditions.

A vector-control-based scheme is used to meet the three objectives mentioned above. The control scheme is based on a synchronously rotating dq reference frame, in which the generator current vector and d-axis are always aligned, as shown in Fig. 2.4. The overall control architecture used for the system is as shown in Fig. 2.5. Since the same machine current flows via VSI, IG, and the grid, it is used. The machine currents I_a , I_b , and I_c are sensed and are converted to I_α and I_β using Clarke's transformation. Using I_α and I_β , the θ and unit vectors that are needed for all the subsequent transformations are extracted.

In all the three phases, the machine voltages (i.e., the voltage across the windings of the IG) are sensed and filtered (to remove high-frequency switching harmonics). These components are referred to as V_{ma} , V_{mb} , and V_{mc} which are then converted to $V_{m,d}$ and $V_{m,q}$ using Park's transformation. The V_{in} vector (i.e., the vector which contains information about the vector difference between generator and grid voltages) is found, and the magnitude of this vector $|V_{in}|$ is generated using peak extraction block. The peak extraction block is implemented using Eq-2.6. Scaling by a factor of $\left(\frac{3}{2}\right)$ is done here in order to accommodate Clarke's transformation factor. Then a comparison is made between $|V_{in}|$ and the q-component of machine voltage ($V_{m,q}$), and the error is processed by a PI controller whose output provides the q-axis reference voltage ($V_{q,ref}$) . This voltage represents the voltage that the VSI has to provide to compensate for the reactive power requirement of the IG successfully.

The voltage across the capacitor, which acts as a DC source to the VSI, must be constant for our reactive power compensation scheme to work. In practical cases, the voltage across the capacitor will reduce due to losses in the capacitor and inverter. So, in such cases, a small amount of active power must be drawn from the VSI to maintain the capacitor voltage at a desired constant level. A closed-loop control scheme is employed for this purpose in which the error between the $V_{cap,actual}$ and $V_{cap,ref}$ is fed to a PI controller, whose output provides the d-axis reference voltage ($V_{d,ref}$) for the VSI switching.

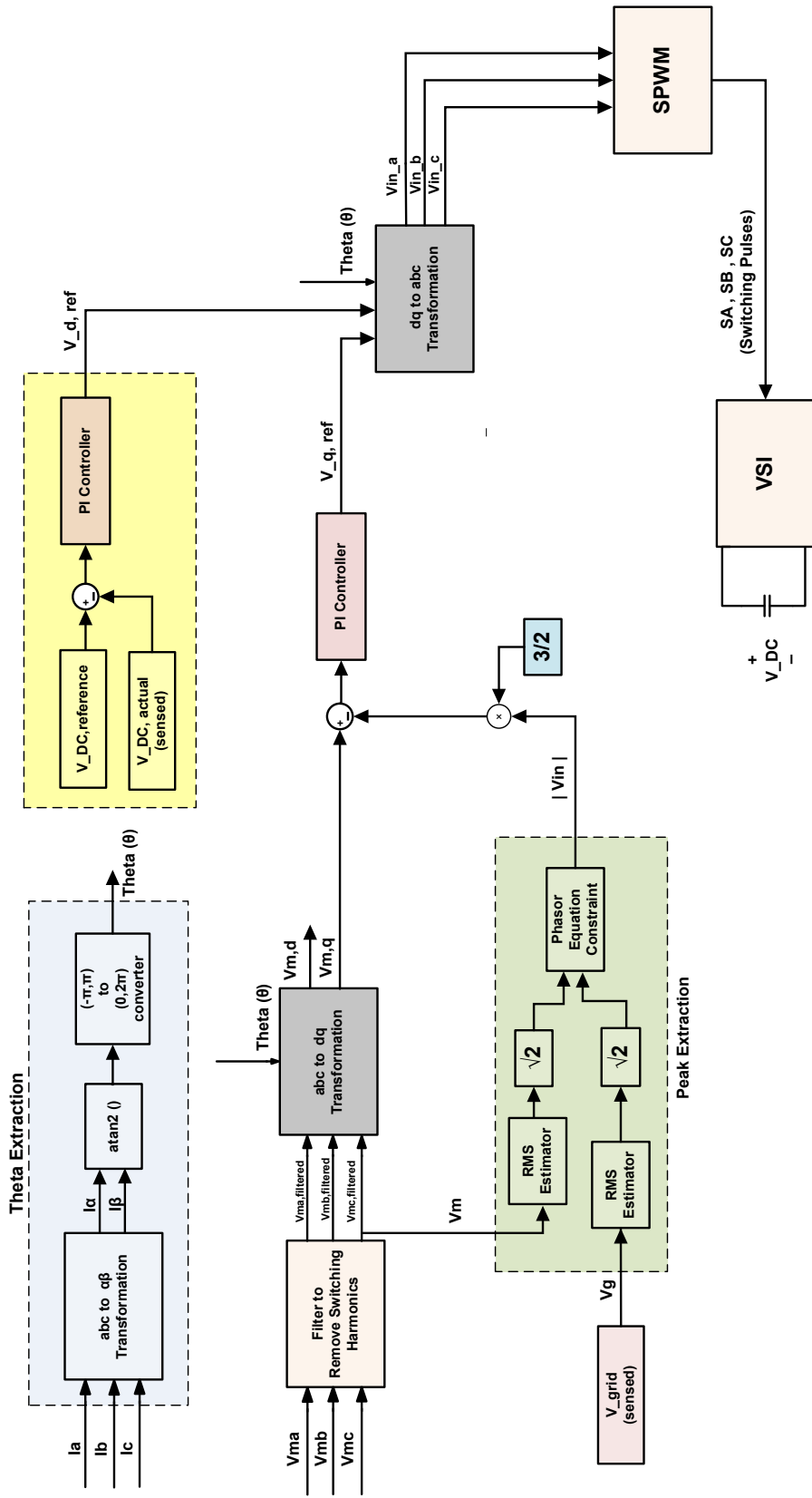


Figure 2.5: Overall control architecture used for series compensation of grid connected IG system.

This component represents the small amount of active power that the VSI draws to maintain constant DC link voltage. $V_{q,ref}$ and $V_{d,ref}$ are then transformed back to three-phase modulating reference voltages using inverse Park's transformation . The obtained $V_{in,a}$, $V_{in,b}$, and $V_{in,c}$ are fed to a conventional sinusoidal pulse width modulation (SPWM) module [17] to generate the switching pulses to drive the VSI. In SPWM, the peak value of the fundamental component of the VSI phase voltage is given by: $V_{in,peak} = \frac{m \cdot V_{DC}}{2}$. Here ‘m’ is the modulation index, usually set around 0.7-0.8. The value of capacitance to be used will be based on the voltage ripple requirements, and this, in turn, depends on the VSI current and frequency of switching (f_{sw}).

2.4 Reactive Power Compensation for Grid and Load

Connected IG system using series STATCOM

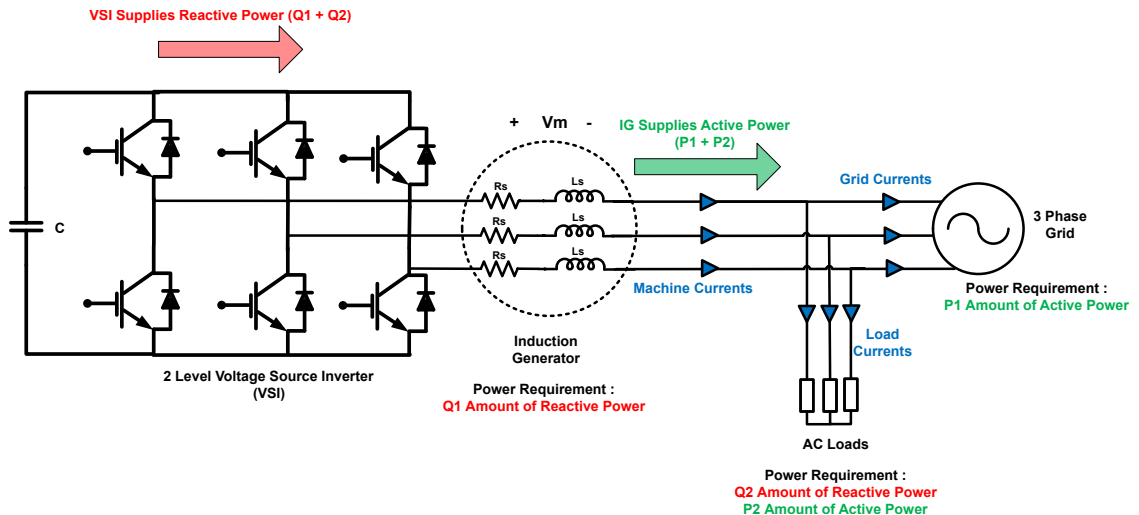


Figure 2.6: Circuit diagram for the series compensation of grid and load connected system.

In the grid plus load connected IG system with series compensation , one side of the stator windings is connected to a capacitor fed VSI as shown in Fig. 2.6, while the other is connected directly to the grid and loads. Since a series compensation scheme is used, interfacing inductors between VSI and IG can be avoided, and hence the weight, size, and

losses in the system can be minimized. The machine windings also act as an interfacing inductor between VSI and the loads.

2.4.1 Power Flow in the System

The reactive power required for excitation of the induction generator (Q_1) and the reactive power required by the loads (Q_2) are provided by the capacitor fed VSI. When the prime mover rotates the induction machine at speed greater than its synchronous speed, it will start generating. The induction generator will supply the active power required by the loads (P_2), and a control scheme is implemented to ensure the unity power factor between grid voltage and grid current. UPF operation ensures that only active power (P_1) is supplied to the grid by the induction generator. Since the loads are connected in a shunt manner near the grid, the machine current (I_m) will now split at the grid-load junction into two components. The currents flowing into the loads are referred to as load currents (I_{load}), and currents entering the grid are referred to as grid currents (I_{grid}). To ensure that only reactive power is drawn from the VSI, a control loop has to be employed to ensure that the phase difference between the fundamental component of VSI (V_{in}) and generator current (I_m) is 90° . However, in a practical scenario, the machine will draw a small amount of active power from the VSI to compensate for the losses in the capacitor and inverter and maintain a constant DC link voltage across the capacitor.

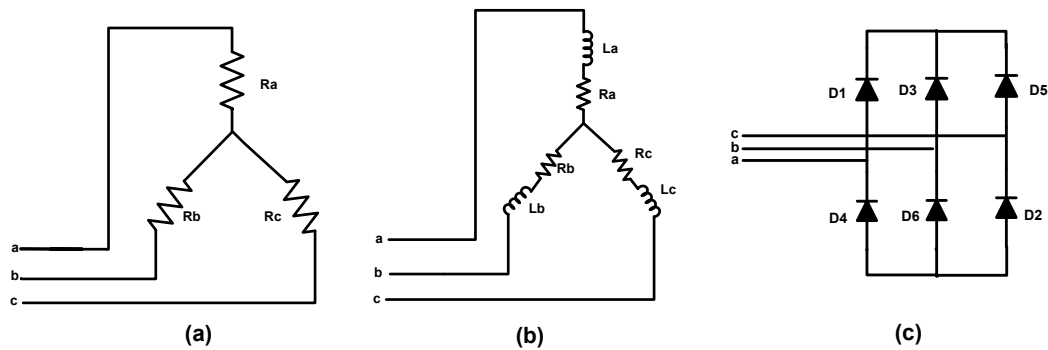


Figure 2.7: (a) Linear Resistive Loads (b) Linear R-L Loads (c) Non-Linear DBR Load. Loads can be either balanced or unbalanced.

The control scheme must support linear (resistive and resistive plus inductive) loads and non-linear DBR kind of loads. For the analysis, the loads are assumed to be star-connected. Fig. 2.7 depicts the various kinds of loads in various scenarios.

2.4.2 Control Architecture used for Grid and Load Connected IG System

The phasor diagram and relation between I_m , V_{in} , V_m , and V_g is straight-forward in this case. The same machine current flows via VSI and IG in the grid-connected system and eventually enters the grid. However, in the case of grid and load connected system, the machine current flows via VSI and IG, and then it splits into load current and grid current. When seen from the node of grid and load, a *leading power factor* is seen. This is because the loads consume both active and reactive power. From the machine side, the system appears as if it is delivering $P_1 + P_2$ amount of active power and Q_2 amount of reactive power. From KCL and KVL, the following relations are known for the phasor quantities:

$$\overrightarrow{I_{machine}} = \overrightarrow{I_{grid}} + \overrightarrow{I_{load}} \quad (2.7)$$

$$\overrightarrow{V_{in}} = \overrightarrow{V_m} + \overrightarrow{V_{grid}} \quad (2.8)$$

The modified phasor diagram (as shown in Fig. 2.8) has been reconstructed based on the following control objectives:

- Maintain a 90° phase shift between V_{in} and $I_{machine}$. This ensures that active power is not supplied from the VSI.
- Maintain Unity Power Factor (UPF) at grid end, i.e., V_{grid} and I_{grid} must be in phase. This ensures that only active power is transferred between IG and the grid, and no reactive power flow happens between them.

- To maintain a constant voltage across the capacitor of the VSI under all operating conditions.

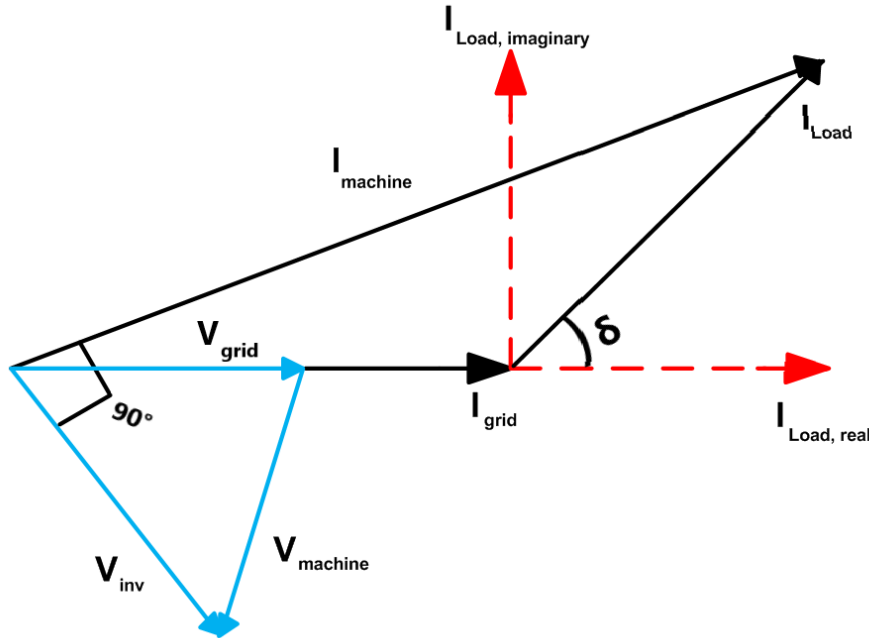


Figure 2.8: Phasor Diagram in case of grid and load connected IG system with Series Reactive Power Compensation.

In the grid-connected case, the currents entering the grid and machine currents were the same, but in the grid and load connected case, the machine current is not equal to the grid current, and they are related as per Eq-2.7. The only change in the control block implementation as compared to the earlier grid-connected system is that now the currents entering the grid (I_{grid}) have to be sensed rather than the machine currents, which was the case earlier. The grid currents have to be used to generate θ , which will be used for subsequent transformations. The remaining part of the control block implementation remains the same as that of the grid-connected system. The modified overall control scheme for the system is as shown in Fig. 2.9.

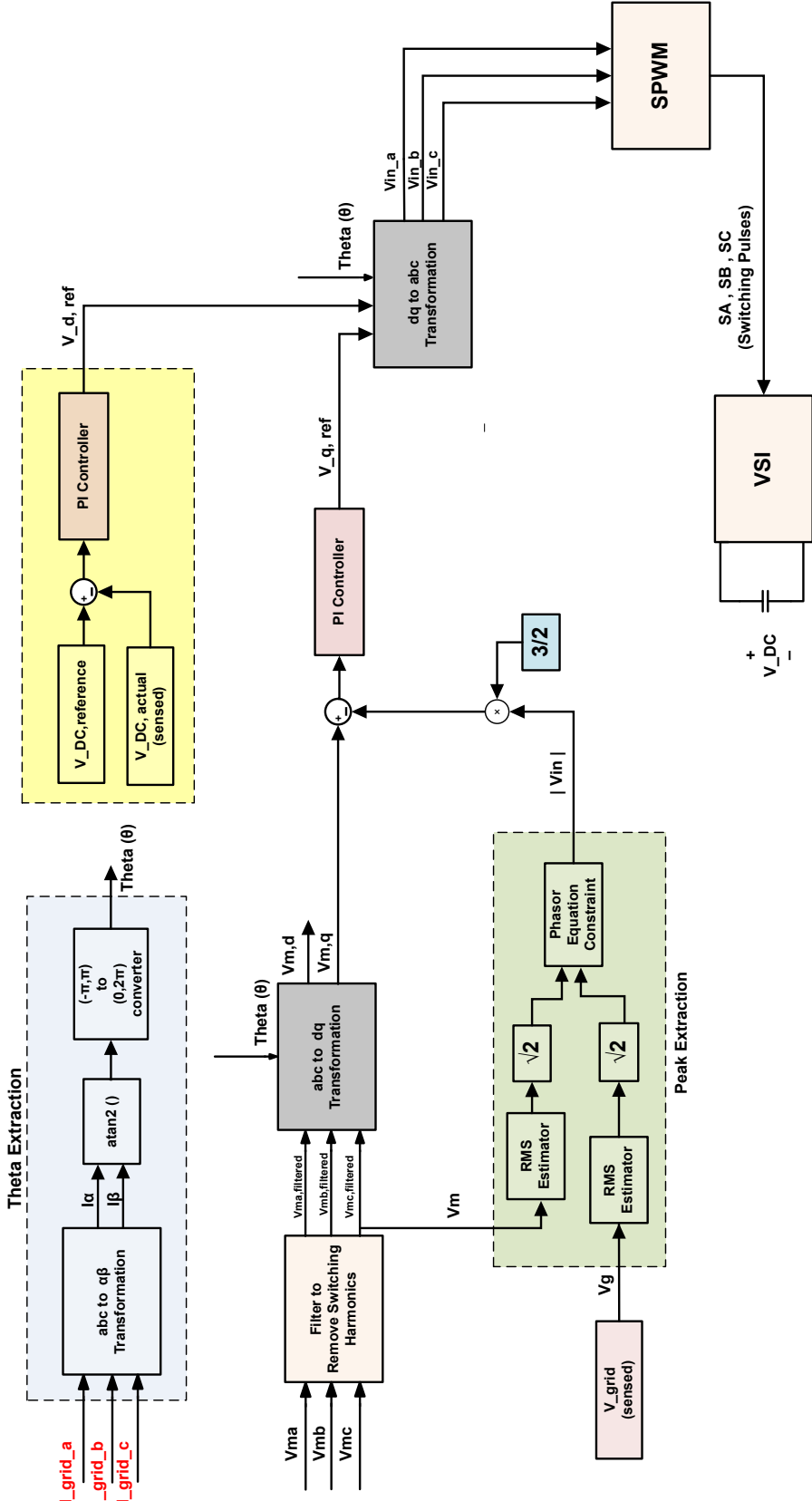


Figure 2.9: Overall control architecture used for series compensation of grid and load connected IG system .

Table 2.2: Difference between Grid Connected, Grid and Load Connected IG Systems

S.No	System	Currents Sensed and Used for θ Extraction
1	Grid Connected IG System with Series Reactive Power Compensation	$I_{\text{machine}} = I_{\text{grid}}$ Sense : I_{machine}
2	Grid and Load Connected IG System with Series Reactive Power Compensation	$I_{\text{machine}} \neq I_{\text{grid}}$ Sense : I_{grid}

2.5 Application to AC Microgrids

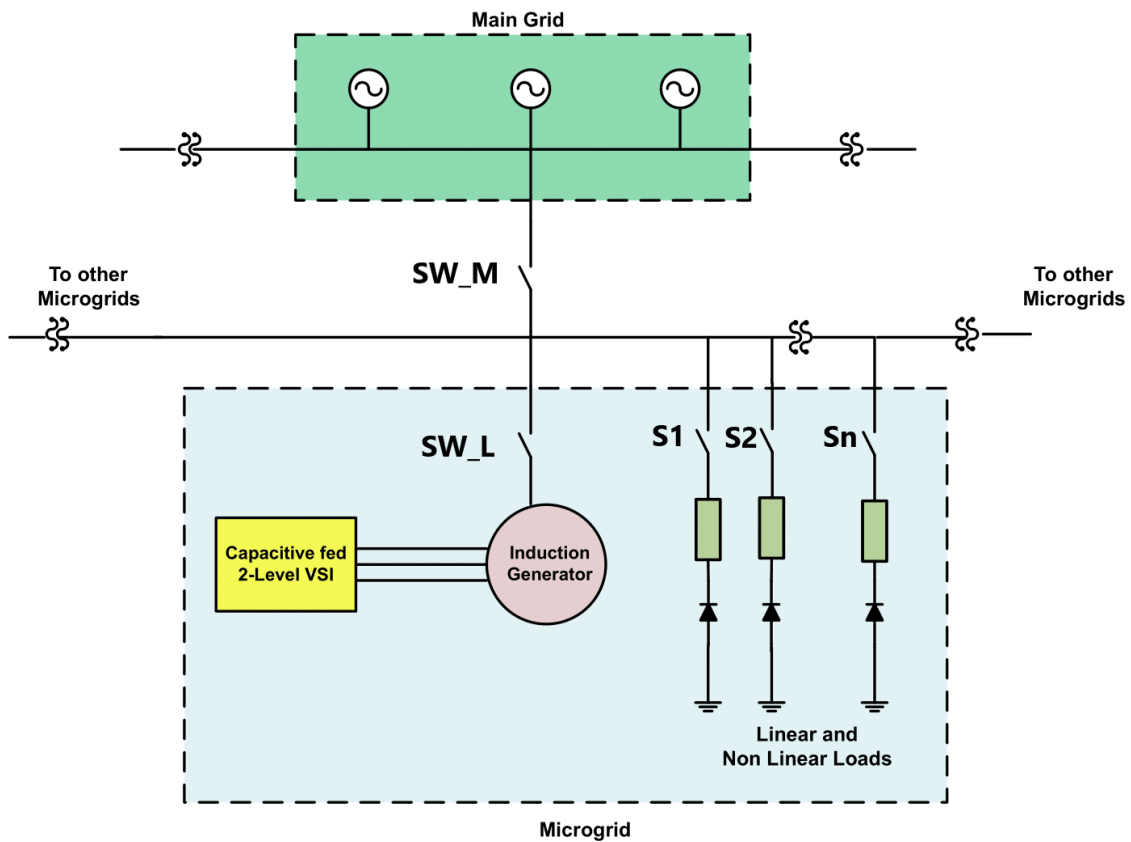


Figure 2.10: Induction Generator based Microgrid Architecture.

"A microgrid is a local energy grid with control capability, which means it can disconnect from the main grid and operate autonomously" [18]. The power within a microgrid can be derived with the help of generators, batteries, or renewable energy sources like windmills, solar panels, etc. In our case, the microgrid is run based on an induction generator. The

Table 2.3: Different Modes of Operation of IG based Microgrid Architecture

S.No	Switch Positions	Mode of Operation	Remark
1	SW_M = Short SW_L = Short S1 = S2 = ... = Sn = Short	Normal Mode of Operation	Architecture is similar to that of Grid and Load Connected IG with Series Reactive Power Compensation
2	SW_M = Short SW_L = Short S1 = S2 = ... = Sn = Open	Generator Mode of Operation	Architecture is similar to that of Grid Connected IG with Series Reactive Power Compensation
3	SW_M = Open SW_L = Short S1 = S2 = ... = Sn = Short	Island Mode of Operation	Microgrid and Main Grid are disconnected. All loads are supported by Microgrid alone.

microgrid and main grid are connected at the point of common coupling (PCC) and maintain the same voltage level as the grid. Whenever there is an emergency or some problem in the main grid the microgrid disconnects from the main grid, and then it operates in an *island mode*.

2.5.1 Power Flow in different modes of operation

2.5.1.1 Normal Mode of Operation

- IG feeds Active Power to Main Grid and Loads.
- VSI supplies reactive power needed for IG excitation and loads.
- If the active/reactive power is not sufficient, then the required extra active/reactive power is drawn from the main grid.

2.5.1.2 Generator Mode of Operation

- IG feeds active power to Main Grid.
- VSI provides the reactive power needed for IG excitation. All the loads are disconnected.

2.5.1.3 Island Mode of Operation

- IG feeds the needed active and reactive power to the loads.
- VSI provides reactive power needed for IG excitation and loads.
- If loads demand more active/reactive power than what VSI and IG can supply, then the power requirements within the local microgrid are not met.

2.6 Conclusion

In this chapter, all the concepts, operation principles, and control schemes for the grid-connected and grid and load connected systems are described in detail. The key differences between the systems are pointed out, and an extension of the grid and load-connected systems to AC microgrids have been presented.

Chapter 3

Simulation Results

3.1 Introduction

This chapter discusses the simulation results of grid-connected and grid-plus-load-connected systems in detail. The simulations were performed in PLECS v4.5.6 software. The main focus of the results is to ensure constant DC link voltage and maintain UPF near the grid for both systems. Additionally, the grid plus load connected system has been simulated under various load conditions, and the results are presented.

3.2 Parameters of the Induction Machine

The induction machine parameters present in the laboratory have been used for simulation purposes. These parameters are summarized in Table 3.1 [14].

Table 3.1: Parameters of IG used during simulation.

S.No	Parameter	Value	Notation
1	Voltage	415V	Rated Phase Voltage
2	Poles	4	
3	Power	11kW	
4	L_m	80 mH	Magnetizing Inductance
5	L_s	2.8 mH	Leakage Inductance of the Stator
6	L_r	2.28 mH	Leakage Inductance of the Rotor
7	R_s	1.05 Ω	Resistance of the Stator
8	R_r	1.98 Ω	Resistance of the Rotor
9	F	1 N	Friction
10	J	0.1 kg.m ²	Inertia

3.3 Simulation Results for Series Reactive Power Compensation of Grid-Connected IG

3.3.1 Setting up the IM in Generator Mode

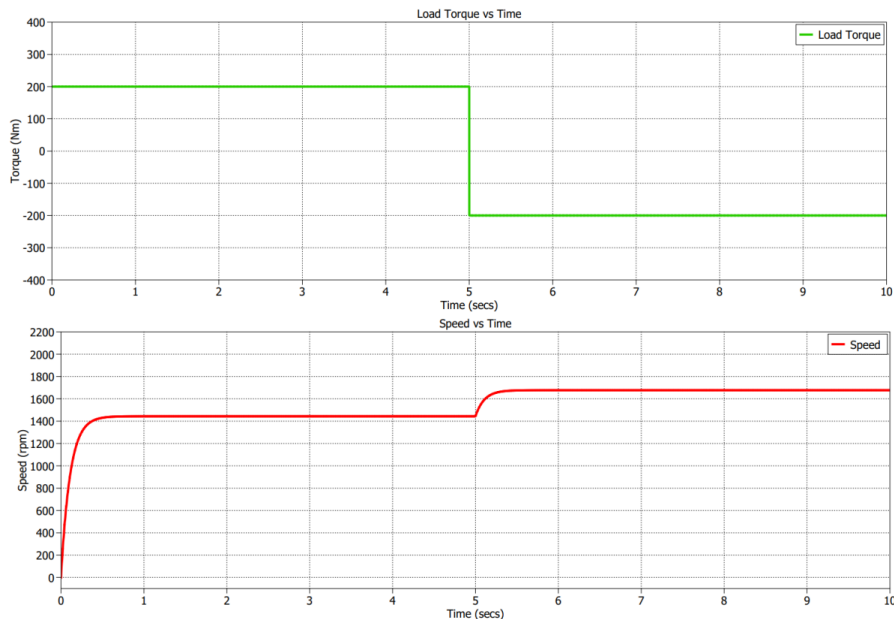


Figure 3.1: Load Torque and Speed Characteristics of the system. At $t=5$ secs, system transits from motoring to generation mode. $\omega_{r,generatingmode} = 1680$ rpm $> \omega_s = 1440$ rpm.

- The induction machine is initially run in motoring mode till $t = 5$ secs by applying a load torque of +200 Nm. At $t = 5$, the load torque is changed to -200 Nm, setting the system into generation mode.
- An IM runs in generator mode when $\omega_r > \omega_s$. In our case, the synchronous speed is 1440 rpm, and in generation mode, the rotor is driven at 1680 rpm. These results are shown in Fig. 3.1.

3.3.2 Phase Reversal in Stator Currents

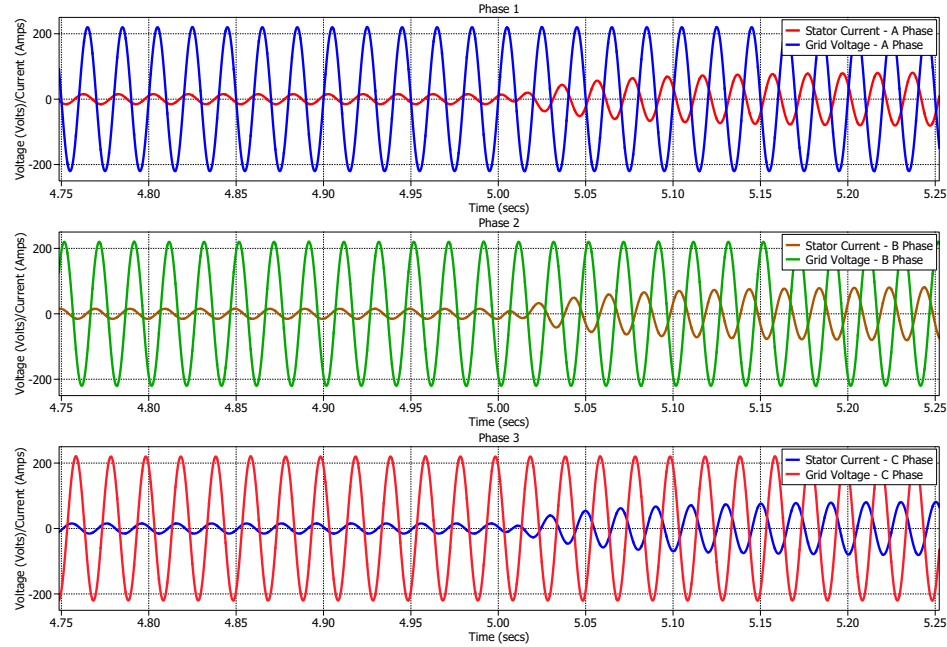


Figure 3.2: Phase reversal (180° flip) in stator currents can be observed at $t=5$ secs.

- When the induction machine transitions from motoring to generator mode, the direction of power flow in the system reverses. This reversal in the direction of flow of stator current can be noted when the generation action starts.
- In motoring mode, the stator currents flow from the grid into the induction machine.

When the IM starts generating, it will pump power back into the grid. In this case, the current will flow from the induction generator to the grid.

3.3.3 DC Link Voltage

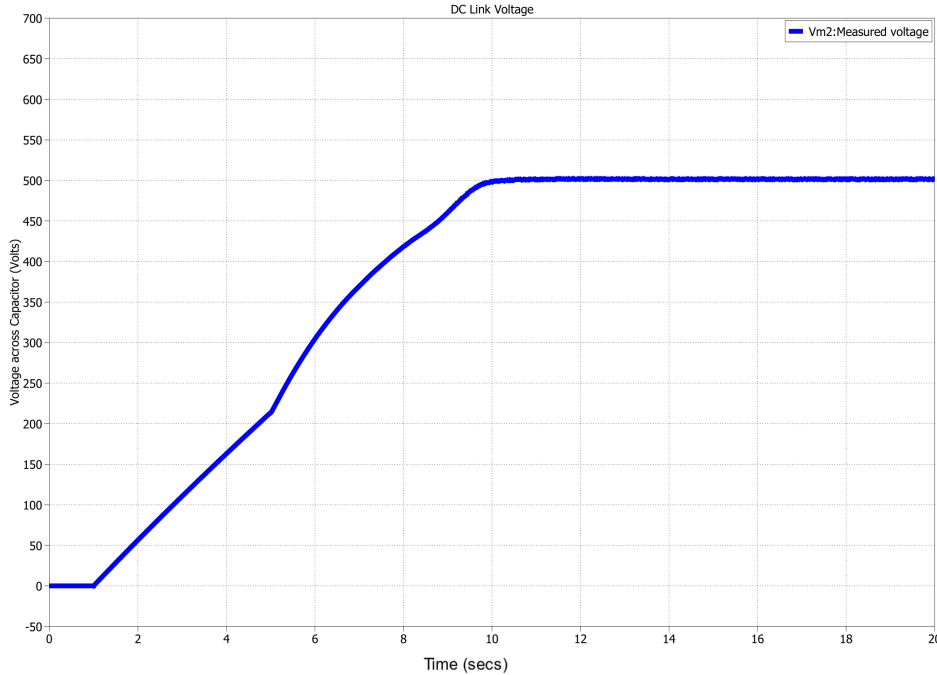


Figure 3.3: DC Link Voltage across the capacitor of VSI ($V_{DC_{ref}} = 500V$ was set during the simulation).

- The designed system works on a vector-control scheme which uses the machine current as reference. So, to generate the reference current vectors and setup the control algorithm, all the top switches (S_1 , S_3 , and S_5) of VSI are shorted till $t = 1$ secs, and later the SPWM is initiated. This is implemented with the help of a small C-script module in the SPWM block.
- A capacitor of 1F is used in the simulation and the DC link voltage plot is obtained as shown in Fig. 3.3. The value of the capacitor while hardware implementation is

expected to be set around 1.1mF , which can be tuned based on the voltage ripple requirements.

- To demonstrate that our system works even without pre-charging the capacitor, an initial condition of 'zero' volts is given to the capacitor. A DC reference voltage of 500 volts is considered, and the error between actual V_{DC} and $V_{DC,ref}$ is given as the input to the PI controller.
- The K_p value is set to 30 , and K_i value is set to 0.005. Such a large value of K_p has been set only to fasten the simulation and make sure it settles within our simulation set up boundaries. A smaller K_p value like 1 can also be used, but the simulation time will be considerably high in this case. The finer the K_i value, the lesser will be our steady-state error. All the appropriate saturation and anti-windup limits have also been set up.

3.3.4 Flow of Active and Reactive Power in the system

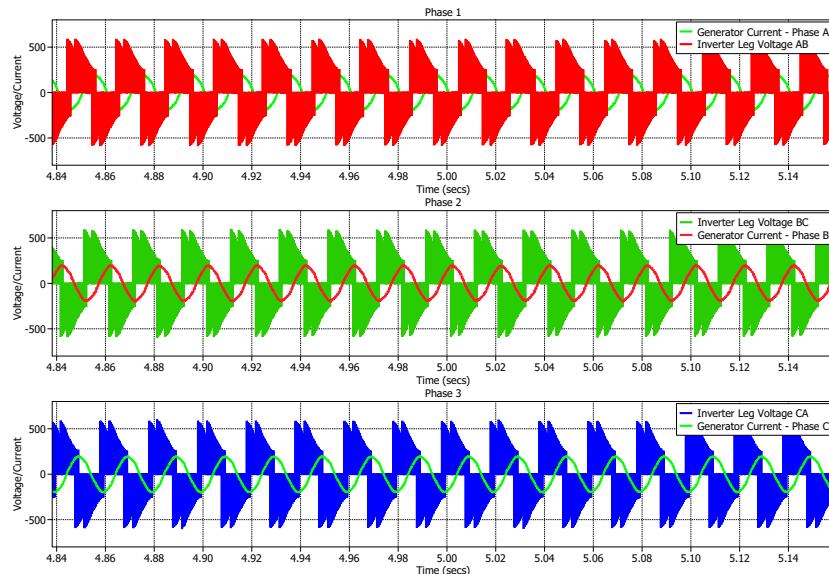


Figure 3.4: Inverter Leg Voltages and Machine Current are approximately 90° phase shifted.

- From Fig. 3.4, it is observed that the inverter leg voltages and machine currents are approximately 90° out of phase.
- From this, it can be concluded that only reactive power (Q) flows between VSI and IG, and VSI can successfully compensate and provide all the reactive power needed by IG for its excitation.

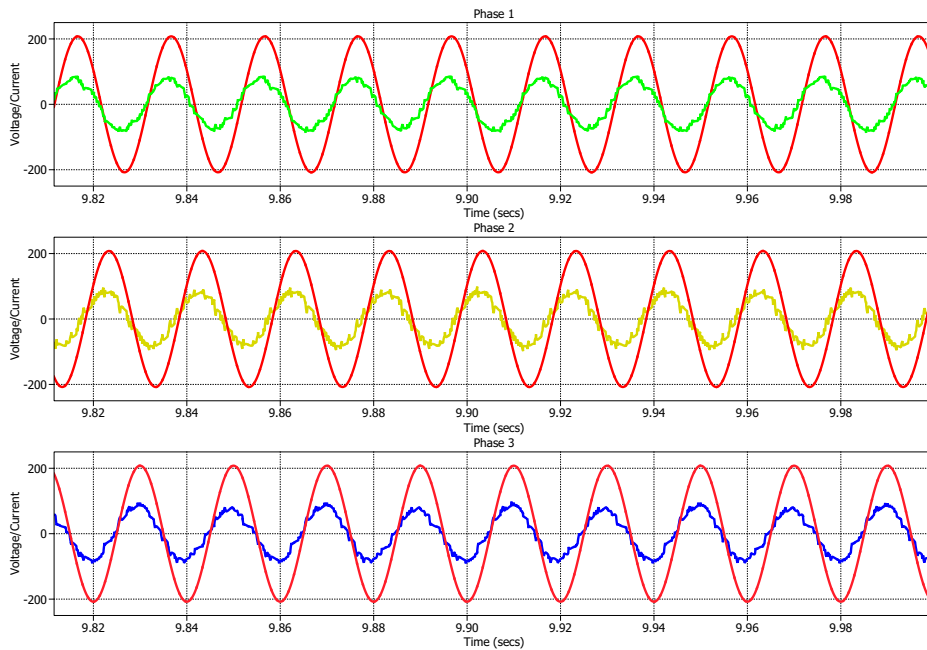


Figure 3.5: Grid Phase Voltage and Grid Currents (entering the grid) are in phase. Plot in red is grid phase voltage and plots in green, yellow, blue are grid phase currents.

- From Fig. 3.5, it is observed that the grid phase voltage and grid phase currents are in phase. From this, it can be concluded that only active power (P) transfer happens between IG and the grid. The IG does not draw any reactive power needed for its excitation from the grid.
- The PI controller employed to ensure UPF has a K_p value of 1.45 and K_i value of 0.09. Filters were not used during this simulation before feeding the machine currents

to the control block. Hence, spikes are seen in the grid current due to the switching harmonics in machine currents. These spikes can be removed by using filters to remove switching harmonics.

3.4 Simulation Results for Series Reactive Power Compensation of Grid and Load Connected IG

The induction machine has been set up in generator mode using the same step torque change as shown in Fig. 3.1. The phase reversal in stator currents is also observed again, as depicted in Fig. 3.2.

3.4.1 DC Link Voltage

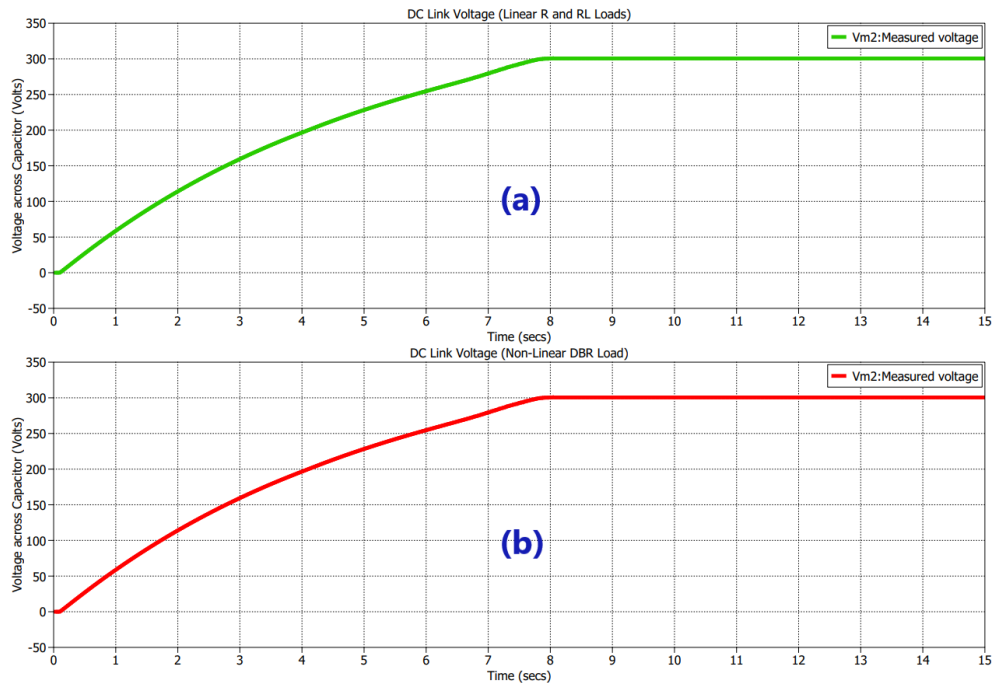


Figure 3.6: DC Link Voltage across the capacitor of VSI for (a) Linear (R and RL Loads) (b) Non Linear DBR Load.

- To generate the reference current vectors and setup the control algorithm, all the top

switches (S_1 , S_3 , and S_5) of VSI are again shorted till $t = 1$ secs (with the help of a C script), and later the SPWM is initiated.

- To demonstrate that our system works even without pre-charging the capacitor, an initial condition of 'zero' volts is given to the capacitor. A DC reference voltage of 300 volts is considered, and the error between actual V_{DC} and $V_{DC,ref}$ is given as the input to the PI controller.
- The DC link voltage reaches the desired value of 300V for all load cases. The simulation was performed for linear R and RL loads in balanced and unbalanced conditions. The value of R used is 10Ω and L used is 2 mH . The DC link voltage stabilizes to 300V even for a non-linear DBR load. The results are as shown in Fig. 3.6.
- The K_p value is set to 30, and K_i value is set to 0.005. All the appropriate saturation and anti-windup limits have also been set up.

3.4.2 Flow of Active and Reactive Power

3.4.2.1 Linear Resistive (R) Loads

- For the simulation, a 3-phase star connected purely resistive load is considered with $R_a = R_b = R_c = 10 \Omega$. The results are first obtained for a balanced load case and then an unbalanced load case is simulated with $R_c = 5 \Omega$, and $R_a = R_b = 10 \Omega$. The DC link voltage is maintained at 300V using the PI controller.
- For purely resistive load case, I_{load} contains only the real part of the current, and the loads consume only active power. This corresponds to the case where $\delta = 0$ in Fig. 2.8.
- The PI controller employed to ensure UPF in all the load scenarios has a K_p value of 1.45 and K_i value of 0.09.

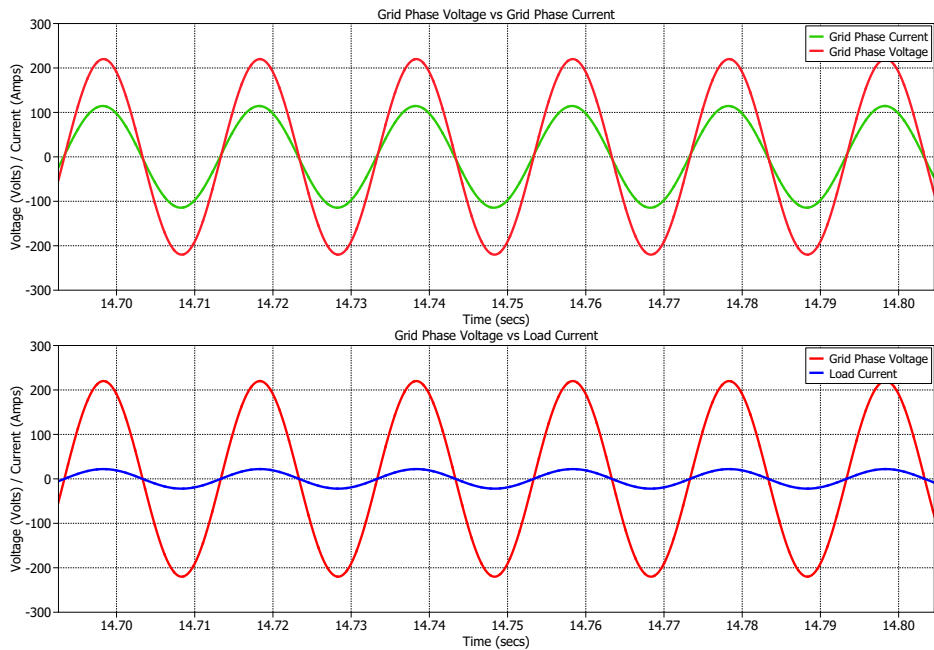


Figure 3.7: Simulation Results for balanced R Load.

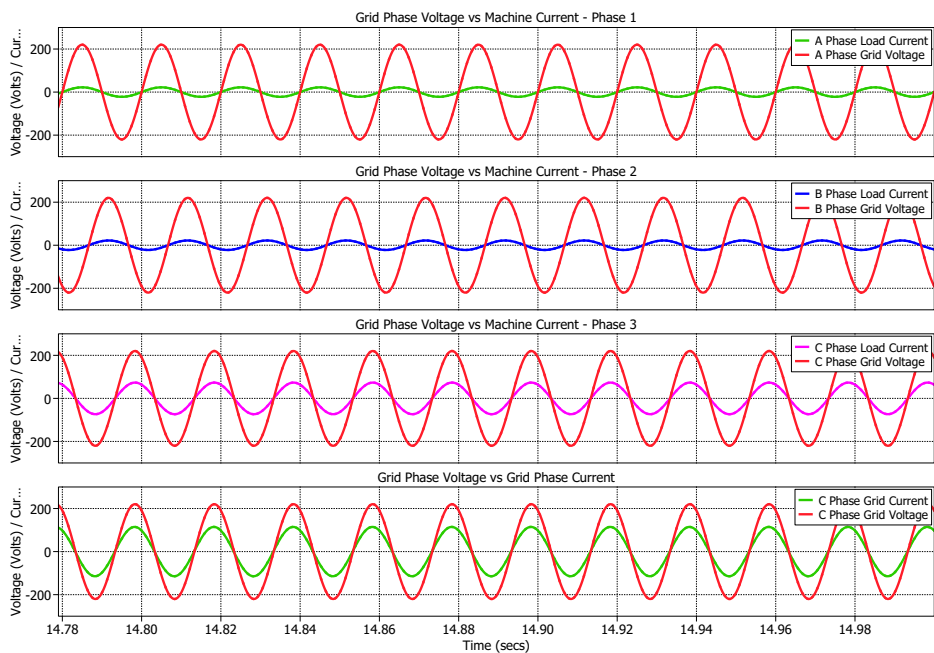


Figure 3.8: Simulation Results for unbalanced R Load.

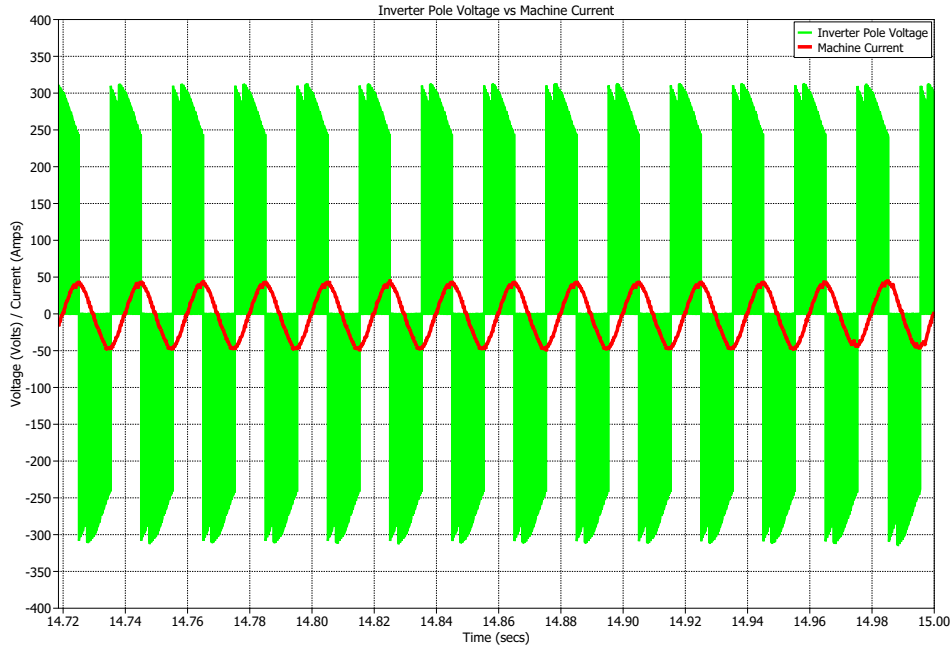


Figure 3.9: Inverter Pole Voltage and Machine Current plot for both balanced and unbalanced R Load cases.

- The load currents in both balanced and unbalanced cases are in phase with the grid phase voltage. This can be observed in Fig. 3.7 and Fig. 3.8. In both cases, the grid phase voltage and grid phase current are in phase, ensuring Unity Power Factor near the grid.
- The reactive power needed for the IG excitation is supplied by the VSI, and this is observed from the 90° shift between machine current and inverted pole voltage in Fig. 3.9.

3.4.2.2 Linear RL Loads

- A 3-phase star connected RL load is considered with $R_a = R_b = R_c = 10 \Omega$, and $L_a = L_b = L_c = 2 \text{ mH}$. The results are first obtained for a balanced load case and then an unbalanced load case is simulated with $R_a = 5 \Omega$, $R_b = R_c = 10 \Omega$, and $L_a = L_b = L_c = 2 \text{ mH}$. The DC link voltage is maintained at 300V using the PI controller.

- For the RL load case, I_{load} contains both real and imaginary parts. Hence, the loads will consume both active and reactive power. This corresponds to the case where $\delta > 0$ in Fig. 2.8.
- The load currents in both balanced and unbalanced cases maintain a leading power factor with respect to the grid phase voltage. This can be observed in Fig. 3.10 and Fig. 3.11. In both cases, the grid phase voltage and grid phase current are in phase, ensuring Unity Power Factor near the grid.
- The reactive power needed for excitation of IG and the loads are supplied by the VSI. This is observed from the 90° shift between machine current and inverted pole voltage in Fig. 3.12.

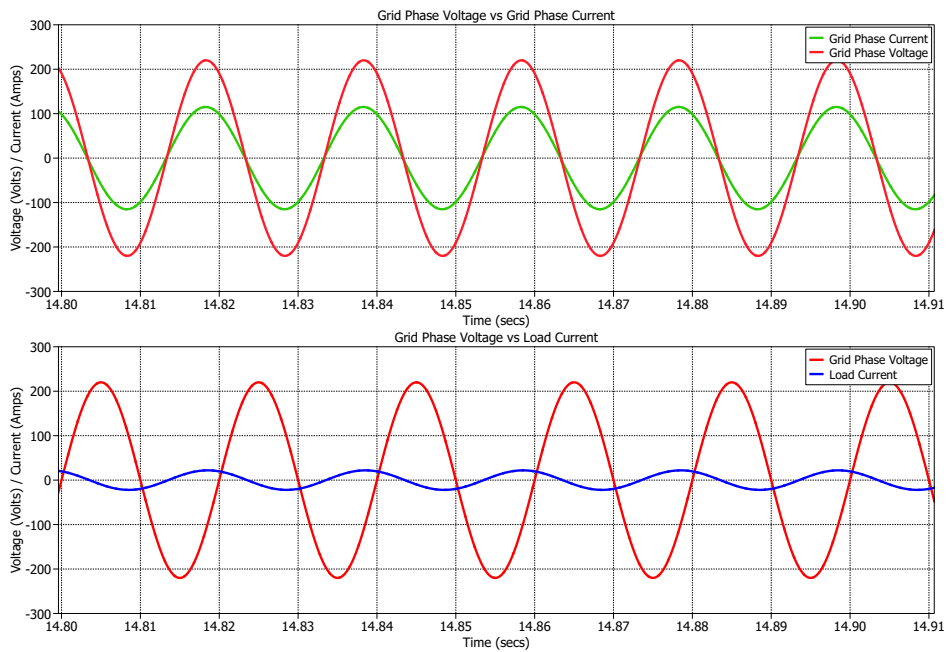


Figure 3.10: Simulation Results for balanced RL Load.

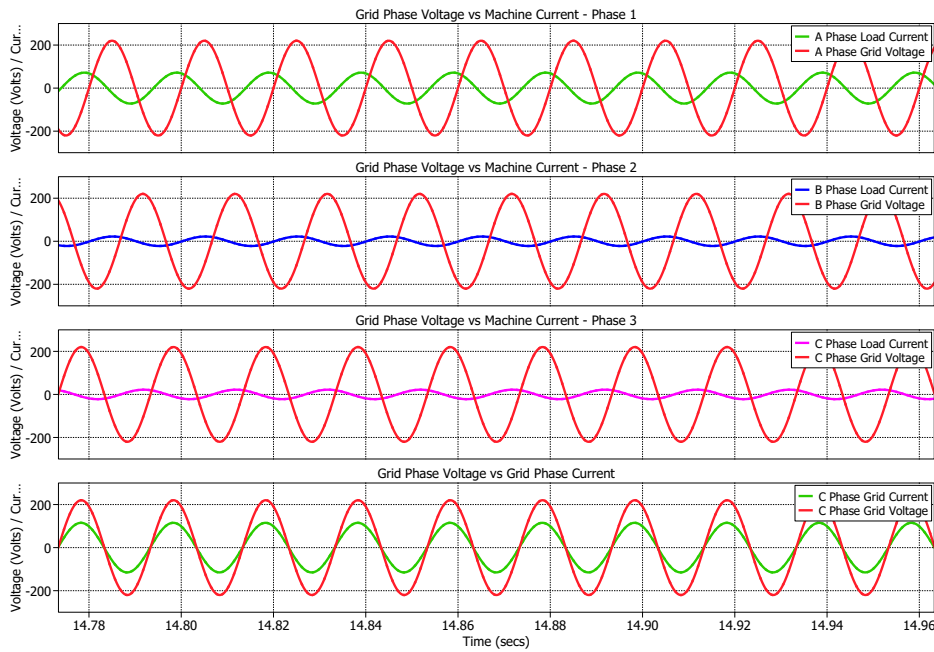


Figure 3.11: Simulation Results for unbalanced RL Load.

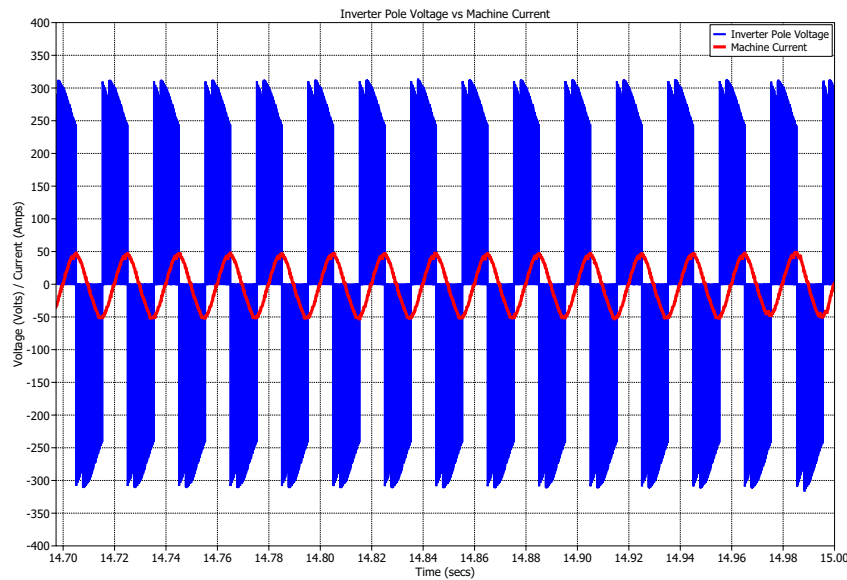


Figure 3.12: Inverter Pole Voltage and Machine Current plot for both balanced and unbalanced RL Load cases.

3.4.2.3 Non-Linear DBR Load

- A 3-phase diode bridge rectifier (DBR) load is connected at the other end of IG windings.

The diodes were configured with a turn-on voltage of 0.7V and an on-resistance of $1 \mu\Omega$. The DC link voltage is maintained at 300V using the PI controller.

- For the non-linear DBR load case, I_{load} contains both real and imaginary parts. I_{load} will also exhibit peaky current nature since the diodes conduct only for some duration in each cycle. The loads may consume both active and reactive power based on the power factor of the non-linear load. In our case, the non-linear load exhibits a leading power factor ($\delta > 0$).

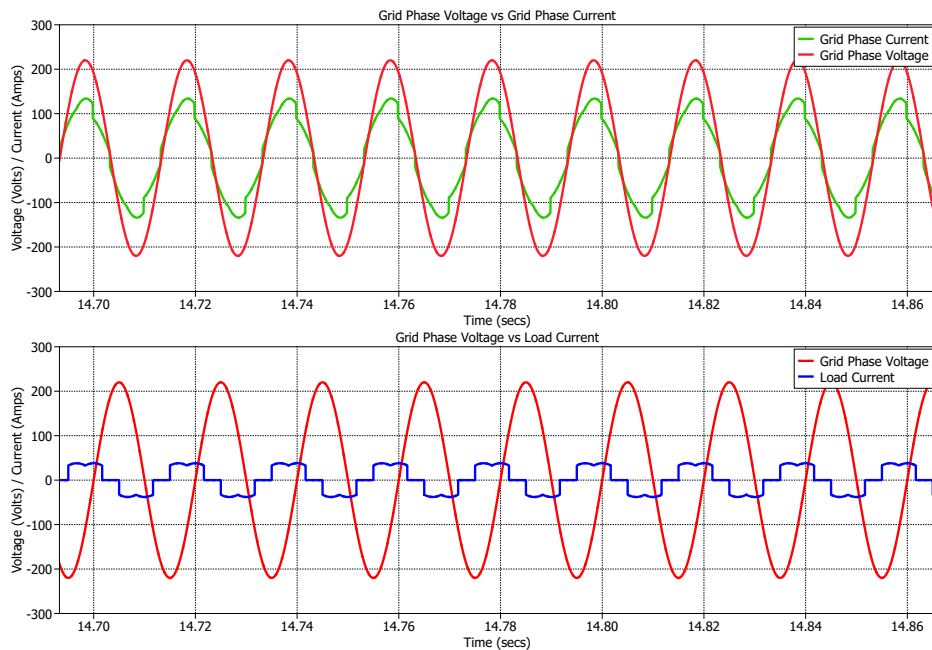


Figure 3.13: Simulation Results for a non-linear DBR Load.

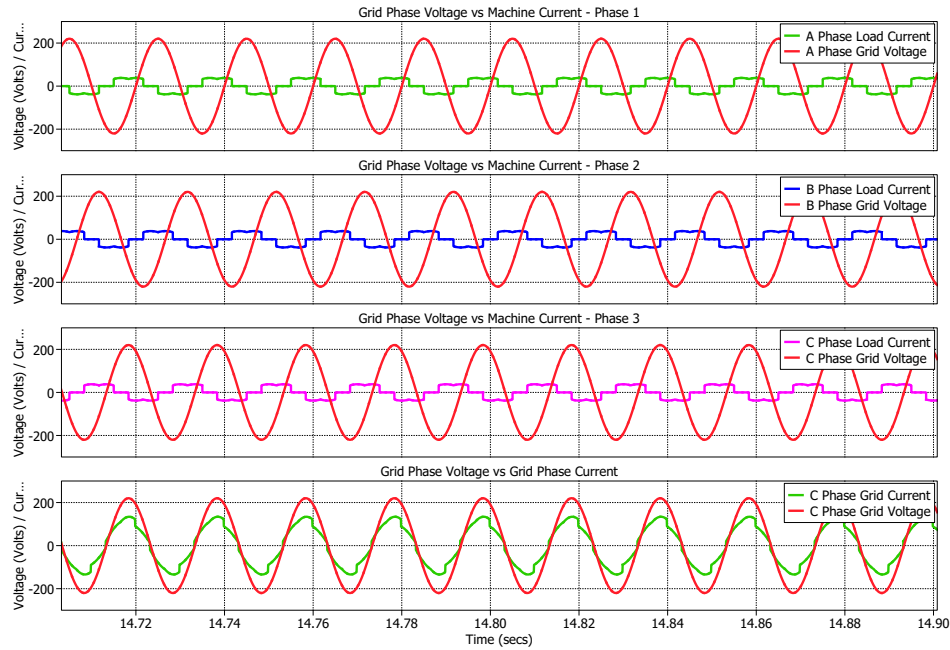


Figure 3.14: UPF being maintained in case of non-linear DBR load .

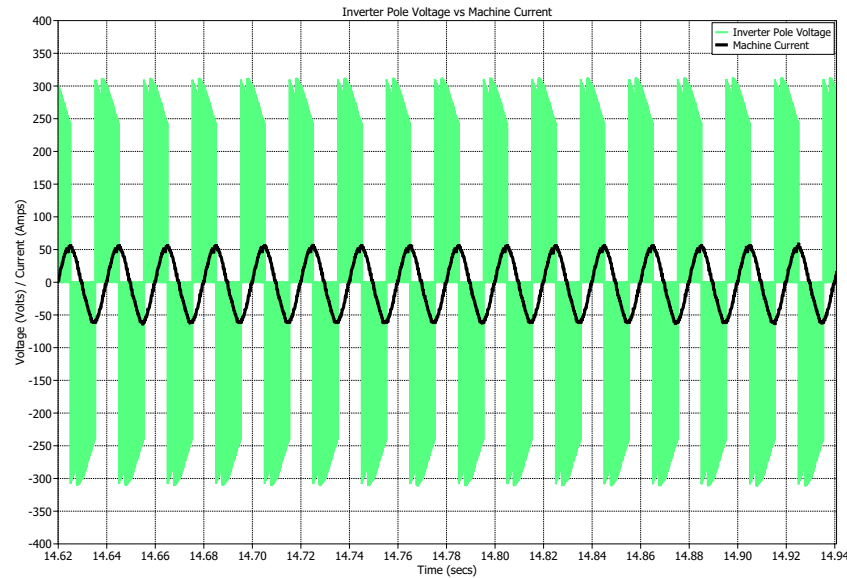


Figure 3.15: Inverter Pole Voltage and Machine Current plot for a non-linear DBR Load case.

- The peaky load currents in both balanced and unbalanced cases maintain a leading power factor with respect to the grid phase voltage. This can be observed in Fig. 3.13 and Fig. 3.14. In both cases, the grid phase voltage and grid phase current are in phase, ensuring Unity Power Factor near the grid.
- The reactive power needed for excitation of IG and the loads are supplied by the VSI. This is observed from the 90° shift between machine current and inverted pole voltage in Fig. 3.15.

3.5 Conclusion

Initially, the series reactive power compensation of grid-connected IG was simulated. The results of DC-link voltage stabilization, UPF near grid, and reactive power transfer from VSI are presented in this chapter. Then the series reactive power compensation of grid and load connected IG was simulated with various linear and non-linear loads under balanced and unbalanced conditions. The results of DC-link stabilization, UPF near grid, and reactive power transfer from VSI to excite IG and loads are presented for all the load scenarios.

Chapter 4

Hardware Modules and Experimental Results

4.1 Introduction

This chapter gives a brief overview of the various hardware modules used for experimental purposes. The experimental results are taken using a step-by-step approach. First, the results showing the implementation of SPWM and reference frame transformations on DSP are discussed. Then the induction machine is configured and run as a generator, and these results are presented. In the later sections of the chapter, the experimental setups and results of series reactive power compensation of VSI are discussed.

4.2 Hardware Modules

The essential modules used for the hardware implementation are :

- Texas Instruments TMS320F28069M DSP Board
- 3- ϕ Auto-Transformer
- Voltage Sensor Board

- Level Shifter Board
- 3- ϕ Inverter
- Hall Effect Current Sensors and Current Probes
- 3- ϕ IG with open-end stator windings
- Diode Bridge Rectifiers
- Differential Probes, DC Supply, Digital Oscilloscopes, and R/L Loads etc.

The 3- ϕ auto-transformer takes the RYB supply (grid) as the input and gives us a controlled 3- ϕ output. The voltage and current sensors work on the Hall-Effect principle, and they sense the required voltages and currents in the system and give them feedback to the DSP for further processing. The level shifter board converts the bipolar signals to unipolar signals within [0,3.3V] to be interfaced with the ADC module on the DSP. The TMS320F28069M DSP module is the central module that does all the processing and implements the required control blocks, filters, etc., for the system. The 3- ϕ inverter in the laboratory comes with an in-built 3- ϕ diode bridge rectifier at the input end. This inverter module contains all the switches (VSI) and the DC link capacitor. A detailed description of each of these modules is given in Appendix A.

4.3 Experimental Results

4.3.1 Implementation of Sine-Triangle PWM on DSP Module

- The TMS320F28069M board was coded to produce and implement the 3-phase SPWM. ePWM modules 1,2,3 were used to produce the switching gate pulses to legs A, B, and C of the inverter.
- Complementary Action Qualifiers were set in the code for ePWM modules 1,2,3 to enable the complimentary pulse generation for top and bottom switches of each leg.

An active high complimentary dead band of 2 μ s (180 clock cycles at 90MHz) was configured in the code to prevent simultaneous turn-on of top and bottom switches in the VSI.

- ePWM module 7 was configured (in DAC mode) to read the digital PWM pulses produced and give the RC filtered output of the pulses. The corresponding sine-wave generated was captured (Fig. 4.3).

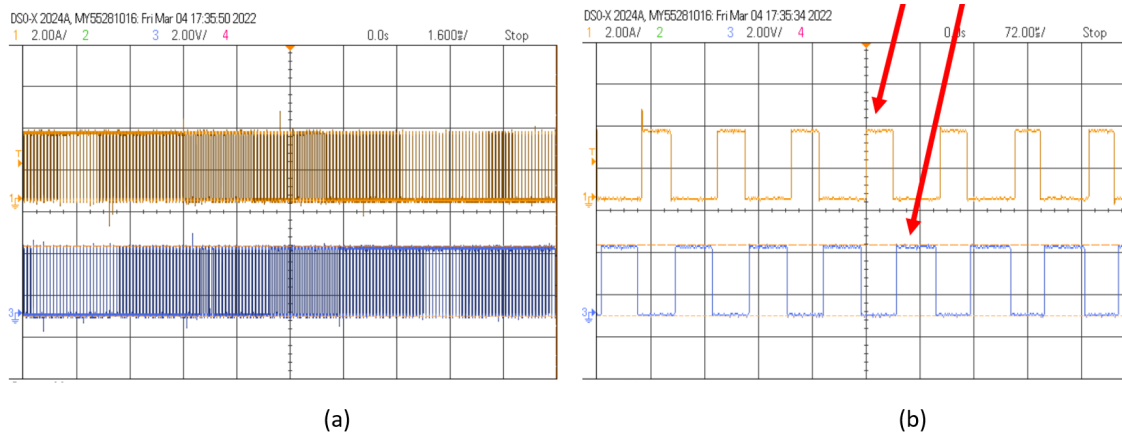


Figure 4.1: (a) Switching Pulses for Top and Bottom Switches of Leg C (Yellow -> Top Switch, Blue -> Bottom Switch) (b) Complementary Switching Pulses generated for Top and Bottom Switches of Leg B (Yellow -> Top Switch, Blue -> Bottom Switch) .

```
Example_2806xAdSoc.c [ Example_2806xEpwmUpDownAQc.c ]
1//#####
2// FILE: Sine_Triangle_PWM.c
4//
5// Monitor ePWM1/2/3/7 pins on an oscilloscope as described
6//
7// Pin Mapping
8//
9// - EPMW1A is on J4-40 (leg A Top Switch)
10// - EPMW1B is on J4-39 (leg A Bottom Switch)
11// - EPMW2A is on J4-38 (leg B Top Switch)
12// - EPMW2B is on J4-37 (leg B Bottom Switch)
13// - EPMW3A is on J4-36 (leg C Top Switch)
14// - EPMW3B is on J4-35 (leg C Bottom Switch)
15// - EPMW7 and 8 are DAC modules
16// - Used to see the SINE Wave output (i.e. digital equivalent of the pulse signals)
17// - EPMW7A is on J4-32 (DAC-1)
18// - EPMW7B is on J4-31 (DAC-2)
19//#####
22// Included Files
24//
25#include "DSP28x_Project.h" // Device Headerfile and Examples Include File
26#include "math.h"
27//
28// Function Prototypes
29//
30//
31void InitPwm1Example(void);
32void InitPwm2Example(void);
33void InitPwm3Example(void);
34void InitPwm7Example(void);
35__interrupt void epwm7_isr(void);
```

```
Example_2806xAdSoc.c [ Example_2806xEpwmUpDownAQc.c ]
310 EPwm1Regs.TBCTL.bit.PHSEN = TB_DISABLE; // Disable phase loading
311 EPwm1Regs.TBCTL.bit.HSPCLKDIV = TB_DIV1; // Clock ratio to SYSCLKOUT
312 EPwm1Regs.TBCTL.bit.CLKDIV = TB_DIV1;
313 //
314 EPwm1Regs.CMPCTL.bit.SHDMODE = CC_SHDMOD;
315 EPwm1Regs.CMPCTL.bit.SHDMODE = CC_SHDMOD;
316 EPwm1Regs.CMPCTL.bit.LOADMODE = CC_CTR_ZERO; // Load on Zero
317 EPwm1Regs.CMPCTL.bit.LOADMODE = CC_CTR_ZERO;
318 EPwm1Regs.CMPCTL.bit.SHDMODE = CC_SHDMOD;
319 EPwm1Regs.AQCTLA.bit.CAU = AQ_SET; // Set PWM1A on event A, up count
320 EPwm1Regs.AQCTLA.bit.CAO = AQ_CLEAR; // Clear PWM1A on event A, down count
321 EPwm1Regs.AQCTLB.bit.CAU = AQ_CLEAR; // Set PWM1B on event B, up count
322 EPwm1Regs.AQCTLB.bit.CAO = AQ_SET; // Clear PWM1B on event B, down count
323 //
324 // Dead Band Inclusion in EPwm1
325 EPwm1Regs.DBTCTL.bit.OUT_MODE = DB_FULL_ENABLE;
326 EPwm1Regs.DBTCTL.bit.POSEL = DB_ACTV_HTC;
327 EPwm1Regs.DBTCTL.bit.IN_MODE = DBB_ALL;
328 EPwm1Regs.DBRD = 500;
329 EPwm1Regs.DBFED = 500;
330 //
331 // Interrupt where we will change the Compare Values
332 EPwm1Regs.ETSEL.bit.INTSEL = ET_CTR_ZERO; // Select INT on Zero event
333 EPwm1Regs.ETSEL.bit.INTEN = 1; // Enable INT
334 EPwm1Regs.ETPS.bit.INTPROD = ET_1ST; // Generate INT on 3rd event
335 }
336 EPwm1Regs.ETSEL.bit.INTSEL = ET_CTR_ZERO; // Select INT on Zero event
337 EPwm1Regs.ETSEL.bit.INTEN = 1; // Enable INT
338 EPwm1Regs.ETPS.bit.INTPROD = ET_1ST; // Generate INT on 3rd event
339 }
340 }
341 void
342 InitEpwm2Example()
343 {
344 }
```

Figure 4.2: CCS Code Implementation of SPWM on DSP Module (a) ePWM Configurations and Initialization (b) Complementary Switching Action Qualifiers (c) Deadband Inclusion.

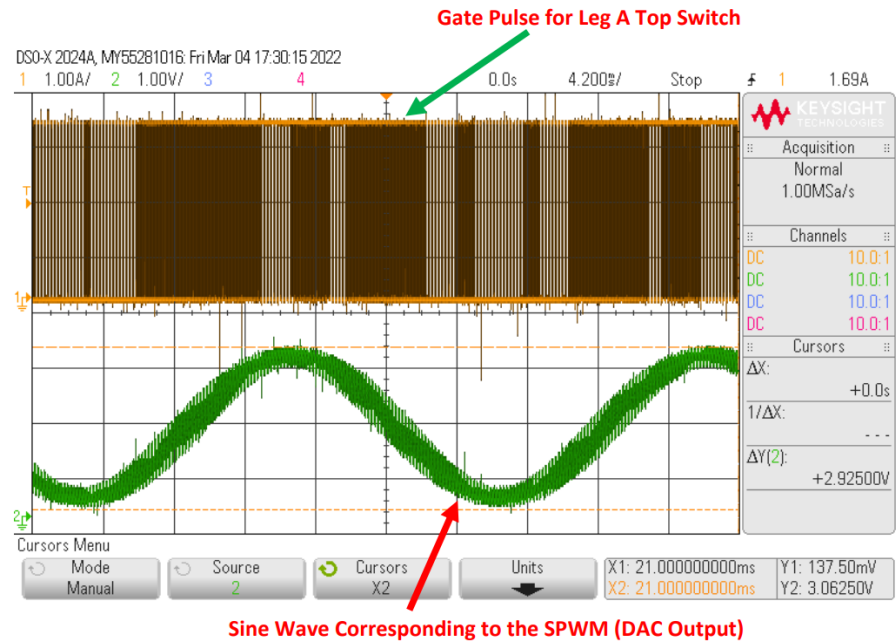


Figure 4.3: Switching Pulses for Leg-A (Yellow) and Sine Output from DAC (Green).

4.3.2 Implementation of Reference Frame Transformations on DSP

Module

- A grid voltage of 170V (peak) was set up from the 3- ϕ auto-transformer output. This voltage was passed to the voltage sensor, followed by the level shifter board.
- The potentiometer on the voltage sensor board was tuned to make the a,b, and c phase voltages at the output of the level shifter fall within the range of [0,+3.3V].
- The output of the voltage sensor, followed by the level shifter module, is as shown in Fig. 4.4.
- The voltage sensor, level shifter, and the ADC board give an undesired offset and gain shift to the sensed signals. Before further processing, these offsets have to be corrected in code. This is shown in Fig. 4.5. Note that these offset values are temperature-dependent and keep on changing.

- The standard Clarke's and Park's transformations are applied to the acquired abc phase signals. The $\alpha\beta\gamma$ and $dq0$ components of the signals are obtained. This is done by writing the transformation matrices in the code as shown in Fig. 4.6.
- The phase angle θ required for the Park's transformation is estimated by implementing a 3- ϕ PLL in the code. The inverse transformations from $\alpha\beta\gamma$ and $dq0$ to abc are also performed in the code.

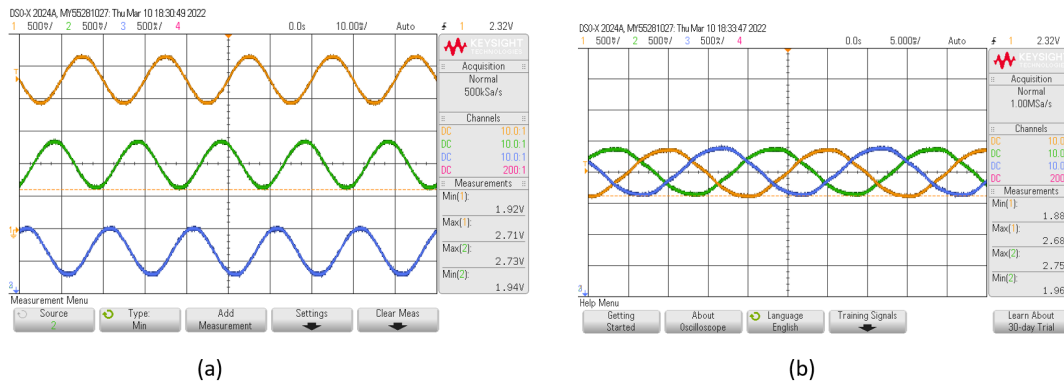


Figure 4.4: O/P of voltage sensor, followed by the level shifter module (a) All phase voltages are within $[0, +3.3V]$ (b) Phases voltages a,b,c 120° phase shifted from each other (Yellow -> A phase, Green -> B Phase, Blue -> C Phase).

```

49 double v_ga=490.51,v_gb=478.29,v_gc=480.68, v_offset_a=2894, v_offset_b=2871, v_offset_c=2885;
50
51 // v_offset_a, v_offset_b, v_offset_c are the offsets in a,b,c phases respectively //
52 // v_ga, v_gb, v_gc are the gain offsets in a,b,c phases respectively //
53
54 double p_a,p_b,p_c,p_alpha,p_beta,pa_ct,pb_ct,pc_ct,p_d,p_q,pa_pt,pb_pt,pc_pt;
55
56 // Dummy Variables used for plotting
57
58 _interrupt void
59 adc_isr(void)
60 {
61     GpioDataRegs.GPBSET.bit.GPIO32 = 1;
62     va = AdcResult.ADCRESULT0;
63     vb = AdcResult.ADCRESULT1;
64     vc = AdcResult.ADCRESULT2;
65
66     // Offset and Gain Correction //
67     // 3.3 V --> means 4096 , so 1 V --> means 1241.212121 . So, divide everything by 1241.2121 ---> same as multiplying by 0.8056e-3 //
68     vas=((va)-v_offset_a)*v_ga*0.8056e-3;
69     vbs=(vb-v_offset_b)*v_gb*0.8056e-3;
70     vcs=(vc-v_offset_c)*v_gc*0.8056e-3;
71
72     // vas,vbs,vcs are the original three phase voltage signals from auto-transformer //

```

Figure 4.5: CCS Code Implementation of Voltage Sensing (a) ADC Data Acquisition (b) Offset and Gain Correction.

```

79 // ****Clarke's Transformations (abc to alpha-beta-gamma) **** //
80
81 v_alpha = (0.6667*vas) - (0.3333*vbs) - (0.3333*vcs) ;
82 v_beta = (0*vas) + (0.5773*vbs) - (0.5773*vcs) ;
83 v_gamma = (0.3333)*(vas + vbs + vcs) ;
84
85 p_alpha = (v_alpha*12.8424) + 2250 ;
86 p_beta = (v_beta*12.4515) + 2250 ;
87
88 // *****Inverse Clarke's Transformations (alpha-beta-gamma to abc) ****//
89
90 va_ct = (1*v_alpha) + (0*v_beta) + (1*v_gamma) ;
91 vb_ct = (-0.5*v_alpha) + (0.8660*v_beta) + (1*v_gamma) ;
92 vc_ct = (-0.5*v_alpha) - (0.8660*v_beta) + (1*v_gamma) ;
93
94 pa_ct = (va_ct*12.6050) + 2250 ;
95 pb_ct = (vb_ct*12.6760) + 2250 ;
96 pc_ct = (vc_ct*12.7768) + 2250 ;
97
98 // *****Park's Transformation (abc to dq0) **** //
99
100 v_d = (0.6667)*(vas*cos(theta) + vbs*cos(theta-(0.6667*PI)) + vcs*cos(theta+(0.6667*PI))) ;
101 v_q = (-0.6667)*(vas*sin(theta) + vbs*sin(theta-(0.6667*PI)) + vcs*sin(theta+(0.6667*PI))) ;
102 v_o = (0.3333)*(vas + vbs + vcs) ;
103
104 p_d = (v_q*-1*25.2808);
105 p_q = v_d;
106
107
108 // *****Inverse Park's Transformation (dq0 to abc) **** //
109
110 va_pt = (cos(theta)*v_d) - (sin(theta)*v_q) + v_o ;
111 vb_pt = (cos(theta-(0.6667*PI))*v_d) - (sin(theta-(0.6667*PI))*v_q) + v_o ;
112 vc_pt = (cos(theta+(0.6667*PI))*v_d) - (sin(theta+(0.6667*PI))*v_q) + v_o ;
113

```

Figure 4.6: CCS Code Implementation for Clarke's and Park's Transformations and their inverse transformations.

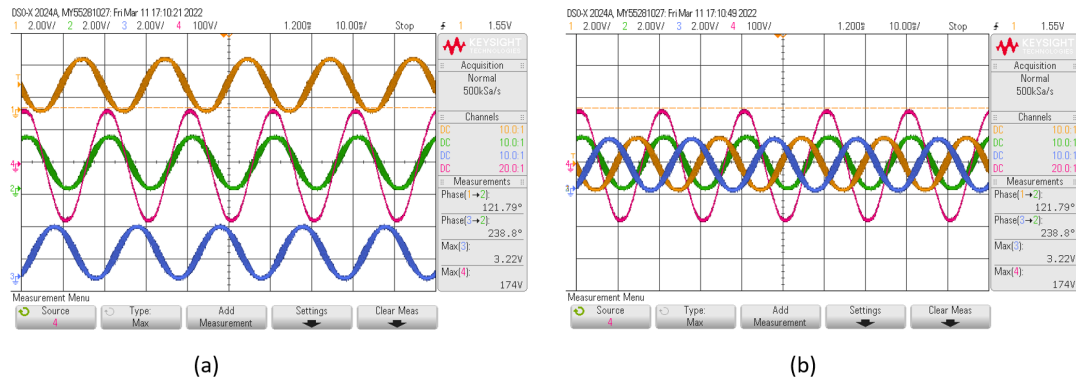


Figure 4.7: V_{abc} phase voltages as sensed and processed by DSP (a) DAC output of V_{abc} and B-phase of grid voltage (b) V_{abc} are 120° phase shifted from each other (Yellow -> A phase, Green -> B Phase, Blue -> C Phase, Pink -> B Phase of Grid Voltage) .

4.3.2.1 Clarke's Transformation

- From Fig. 4.8, it can be noted that V_α and V_a are in phase while V_α and V_β are 90° out of phase. Also the V_α component is around 1.5 times V_a component which is as expected.

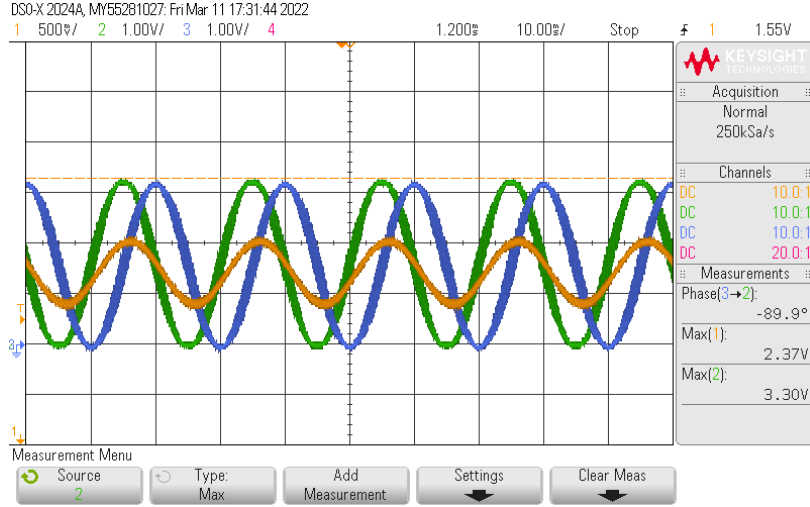


Figure 4.8: $V_{\alpha\beta}$ components of the voltage obtained from Clarke's Transformation (Yellow -> A phase, Green -> α component, Blue -> β component) .

4.3.2.2 Inverse Clarke's Transformation

- The abc components are back-estimated from $\alpha\beta\gamma$ components in the DSP. The obtained results are as shown in Fig. 4.9. It is noted that, V_{abc} are retrieved correctly and they maintain the phase difference of 120° .

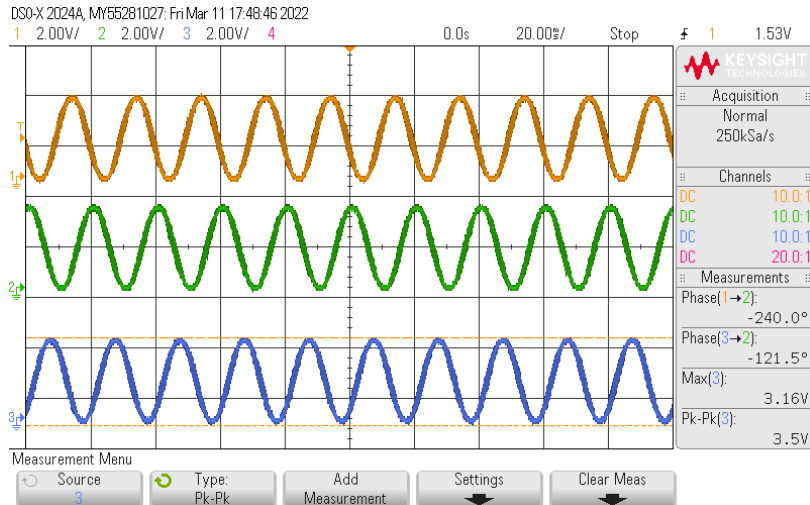


Figure 4.9: V_{abc} components of the voltage obtained from Inverse Clarke's Transformation (Yellow -> A phase, Green -> B phase, Blue -> C phase) .

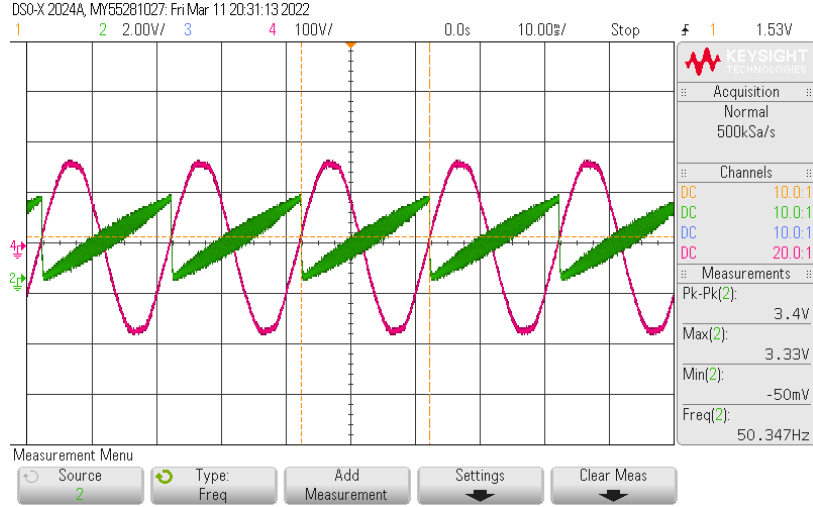


Figure 4.10: θ estimated using the 3- ϕ PLL (Pink \rightarrow A phase of grid voltage, Green \rightarrow θ estimated).

4.3.2.3 Theta (θ) Estimation using 3- ϕ PLL

- The θ value is obtained using a 3- ϕ PLL, in which the error between V_d component and 'zero' is processed using a PLL controller.
- From Fig. 4.10, it is noted that θ has a full range value from $[0, 2\pi]$ and has a frequency of 50Hz (i.e., the grid frequency). The noise in the θ estimate is due to the limitation of the RC filter, which is being used as DAC. An external RC filter can be used to see the more accurate version of θ .

4.3.2.4 Park's Transformation

- Initially, the 3- ϕ signal fed to the dq transformation block was simulated in PLECS under three conditions. In the first phase, both grid voltage and 3- ϕ PLL are off. The grid voltage is turned on in the second phase, but the 3- ϕ PLL is off. And in the final phase, both grid voltage and 3- ϕ PLL are on. The simulation result is as shown in Fig. 4.11.
- The V_d and V_q samples processed by the DSP are collected from the CCS software and imported and plotted via MATLAB.

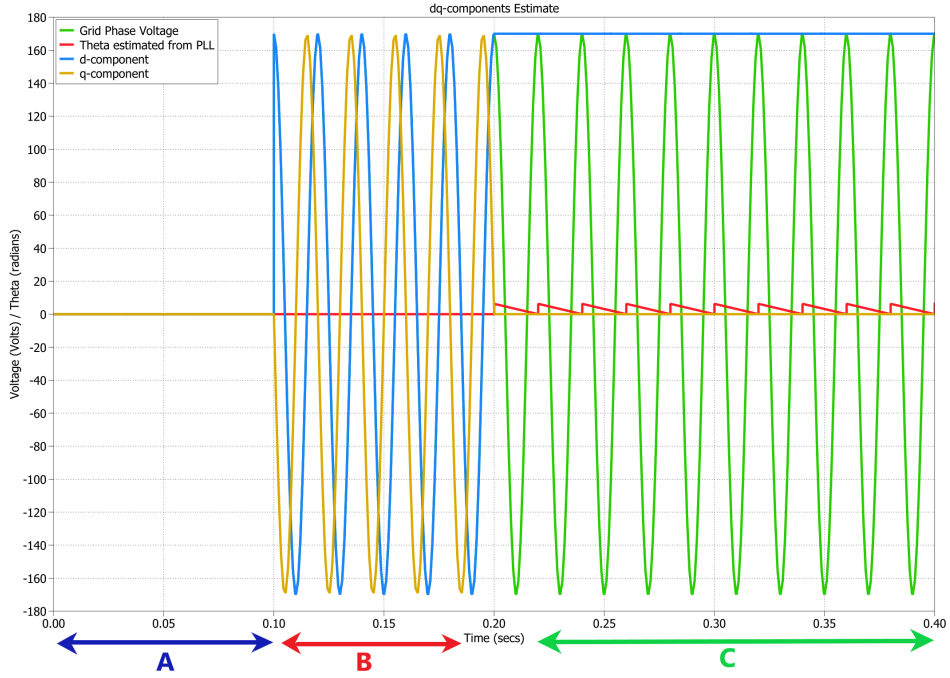


Figure 4.11: V_{dq} components estimated from simulation in PLECS . (A) Grid Voltage, 3- ϕ PLL are OFF, (B) Grid Voltage is ON, 3- ϕ PLL is OFF, (C) Grid Voltage, 3- ϕ PLL are ON .

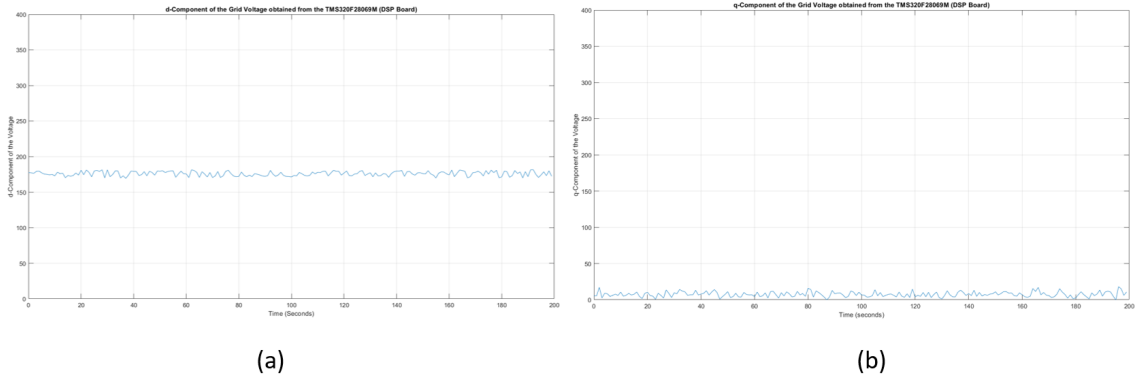


Figure 4.12: V_{dq} components obtained from DSP Module and plotted via MATLAB.

4.3.2.5 Inverse Park's Transformation

- The abc components are back-estimated from $dq0$ components in the DSP. The obtained results are as shown in Fig. 4.14. It is noted that V_{abc} are retrieved correctly, and they maintain the phase difference of 120° .

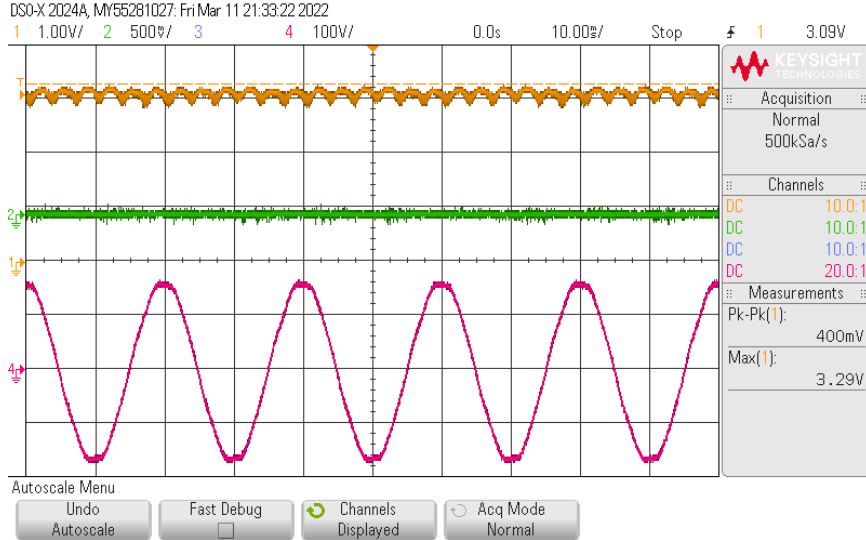


Figure 4.13: V_{dq} components obtained from DSP Module as processed and scaled to +3.3V by DAC (Yellow -> d component, Green -> q component, Pink -> A phase of grid voltage).

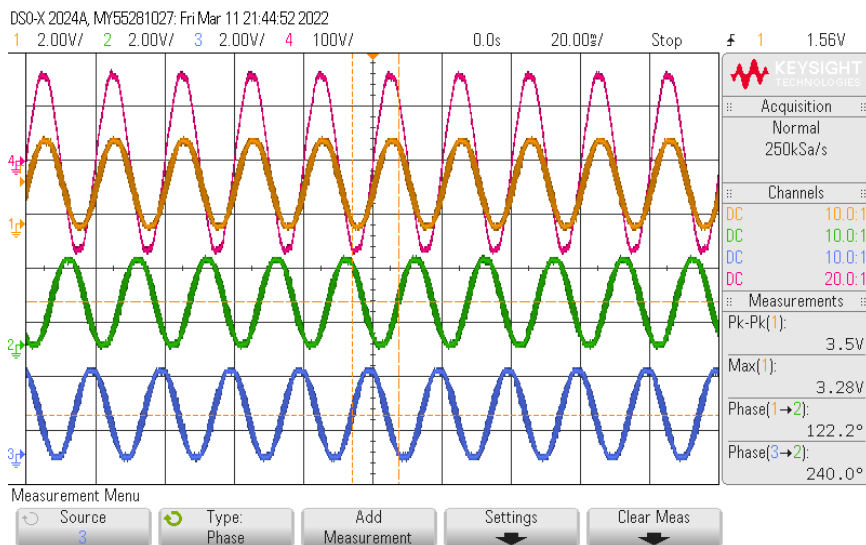


Figure 4.14: V_{abc} components of the voltage obtained from Inverse Park's Transformation (Yellow -> A phase, Green -> B phase, Blue -> C phase, Pink -> A phase of grid voltage) .

4.3.3 Setting up the Induction Machine in Generator Mode

- The induction machine present in the laboratory has a total of 12 terminals starting from A_1, B_1 , up to F_1 on one end, and A_2 to F_2 on the other end.
- This induction machine can be used in the split-phase configuration or simple three-

phase configuration. To operate the machine as a simple three-phase induction machine, the terminals have to be connected, as shown in Fig. 4.15.

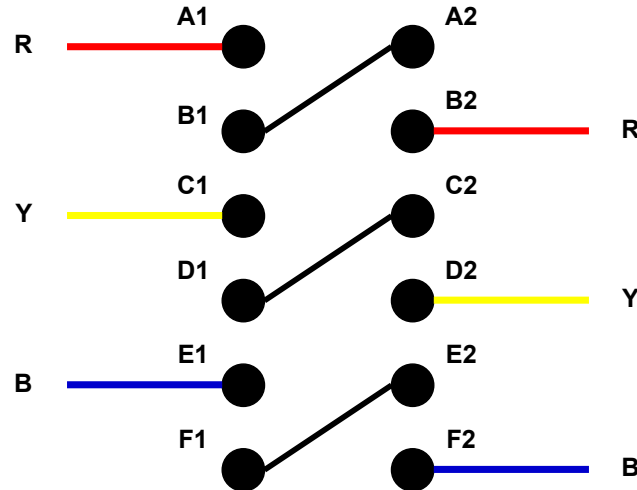


Figure 4.15: Winding configuration used to configure the machine as a 3- ϕ IM.

- To set up the machine in generation mode, the circuit connections are made as shown in Fig. 4.16. First, the *RYB* supply and auto-transformer 2 are turned ON. The diode bridge rectifier (DBR) starts to supply power to the DC motor.
- The knob on auto-transformer 2 is slowly varied from zero to 100V RMS, and the direction of rotation of the DC motor is noted. A rheostat of 10A/10 Ω had to be connected across the armature of the DC motor so that the current flows via the field windings and a sufficient field is developed. Any other DC motor starter technique can also be employed. In our case, a clockwise rotation of the DC motor was observed.
- Then, the auto-transformer 2 is turned off, and auto-transformer 1 is turned ON. The induction machine now starts to take power from the grid, and the DC motor is treated as a load to the IM. The direction of rotation of IM is noted and is found to be counterclockwise.

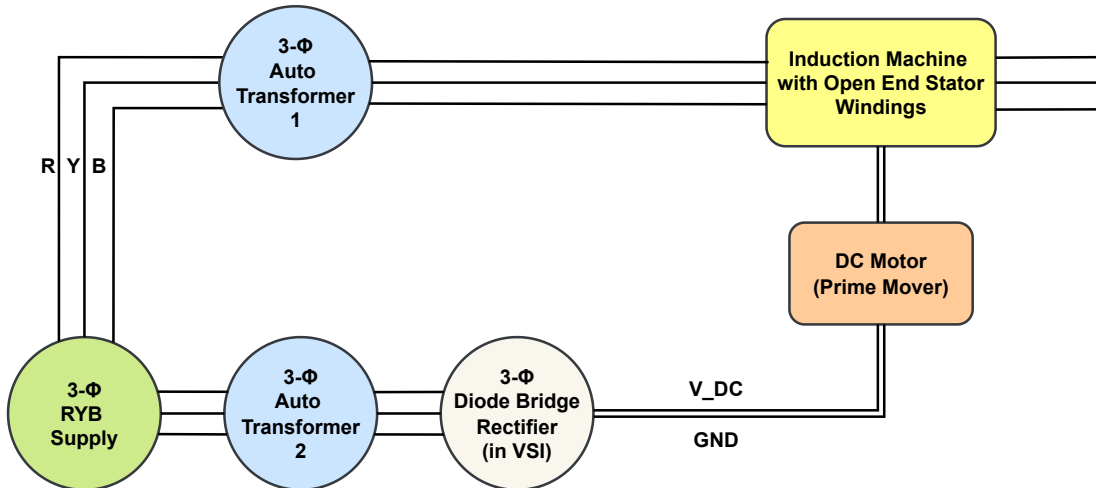


Figure 4.16: Circuit diagram to setup the IM in generation mode.

- The sense of rotation of DC motor and IM must be made the same, i.e., both must be clockwise or counterclockwise. This is done by interchanging the connections of V_{DC} and GND to the DC motor. The same can also be achieved by interchanging any two of the RYB inputs to the IM.
- Then, the IM is powered by auto-transformer 1 alone, and auto-transformer 2 is kept at zero value. Slowly, the auto-transformer 1 knob is increased, and the speed of the IM is noted.
- The grid frequency is 50 Hz, and hence the synchronous speed of the machine would be $\left(\frac{120 \times 50}{4}\right) = 1500$ rpm. In this, the slip is around 60 rpm, and hence the rated speed is 1440 rpm. The auto-transformer 1 is increased till IM reaches synchronous speed.
- Once the IM is at synchronous speed, the auto-transformer 2 is turned on slowly and increased till the speed of IM transitions to just above synchronous speed. Once the IM is above synchronous speed, the IM will start delivering power back to the grid, and a phase reversal can be observed in the stator phase currents. The transition was observed when a V_{DC} of 110V was supplied via the DBR. These results are shown in Fig. 4.17 and Fig. 4.18.

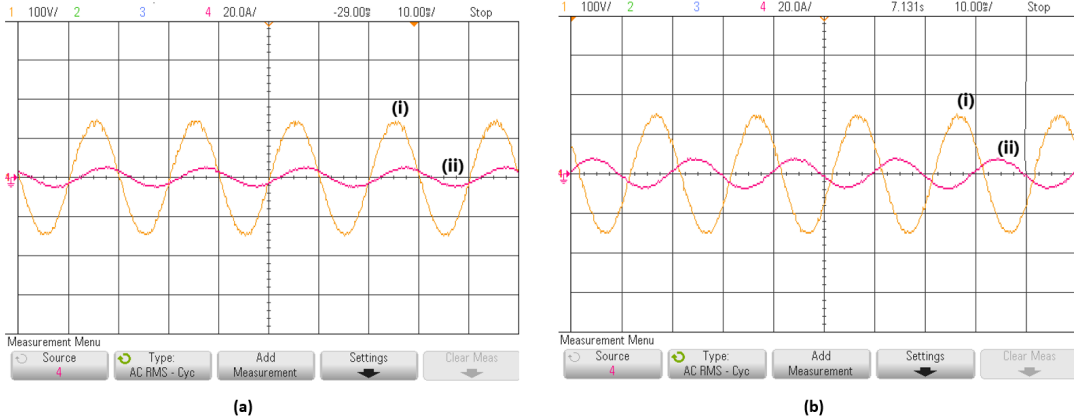


Figure 4.17: (i) Grid Voltage [Y axis: 100V/div] and (ii) Stator Phase Currents [Y axis: 20A/div] in (a) Motoring Mode (b) Generating Mode [X axis: 10ms/div]. Stator Phase currents in both modes are 180° phase shifted.

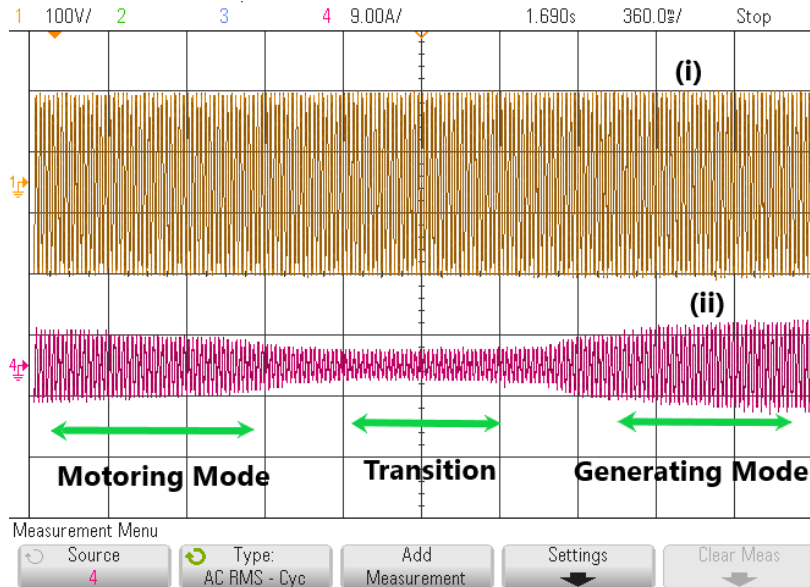


Figure 4.18: Transition from motoring to generating mode [X axis: 360ms/div] (i) Grid Voltage [Y axis: 100V/div] and (ii) Stator Phase Currents [Y axis: 9A/div].

4.3.4 Reactive Power Compensation using VSI

- Until now, when the IM was in generating mode, the required reactive power was taken from the grid. The next step is to supply the required reactive power from a capacitive fed VSI instead of the grid. The circuit diagram for this system is as shown

in Fig. 4.19 and the experimental setup image is as shown in Fig. 4.20 .

- The machine currents are sensed and waves which are 90° phase-shifted to these are used as modulating waves. The modulating waves are generated using a cascade of two - 45° phase shift filters. The filters are implemented on the TMS320F28069M DSP board. Without using the filters, the 90° phase-shifted waves can also be obtained using algebraic methods like Clarke's and Inverse Clarke's transformation.

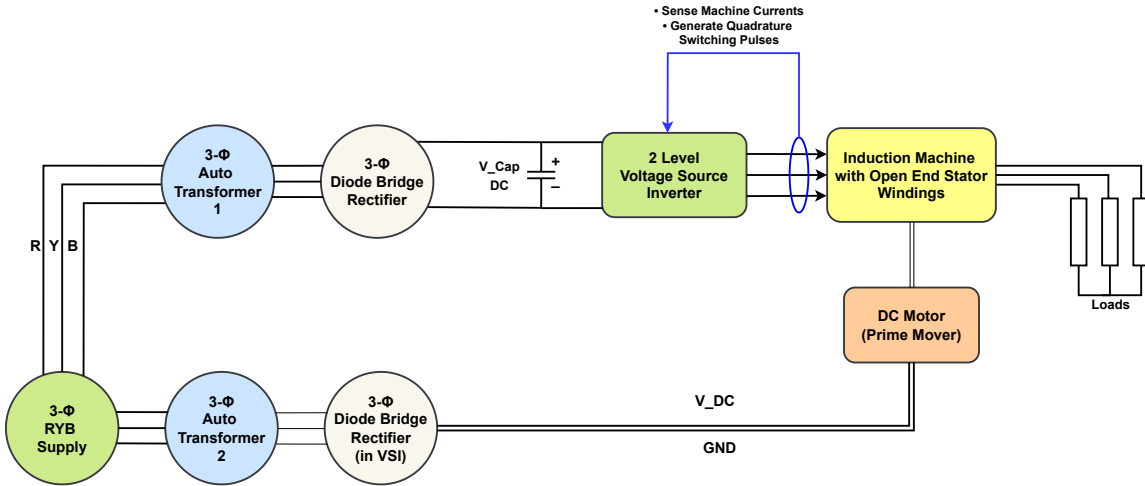


Figure 4.19: Circuit diagram to setup the IM in generation mode with reactive power compensation using VSI.

- These modulating waves are fed to a sine-triangle PWM block in the DSP, and the switching pulses thus generated are fed to drive the VSI. The system is initialized with a 25Hz modulating wave, which sets the synchronous speed to be equal to $\left(\frac{120 \times 25}{4}\right) = 750$ rpm.
- Once the machine starts to operate as a generator, three things are noted. First, a phase reversal in stator phase currents is noted. The current through the rectifier (DBR) near auto-transformer 1 has a peaky profile in motoring mode, while it becomes zero in generating mode. In generator mode, the DC link voltage also increases and settles to our $V_{DC,ref}$ set. These results are shown in Fig. 4.22, Fig. 4.23.

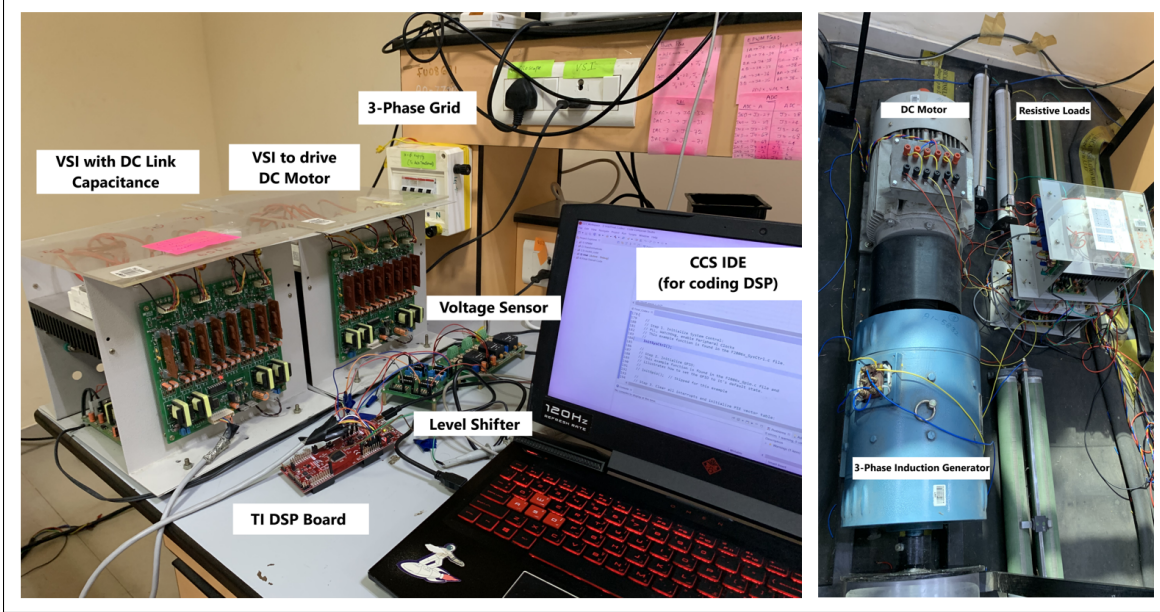


Figure 4.20: Experimental Setup of the IG with reactive power compensation using VSI.

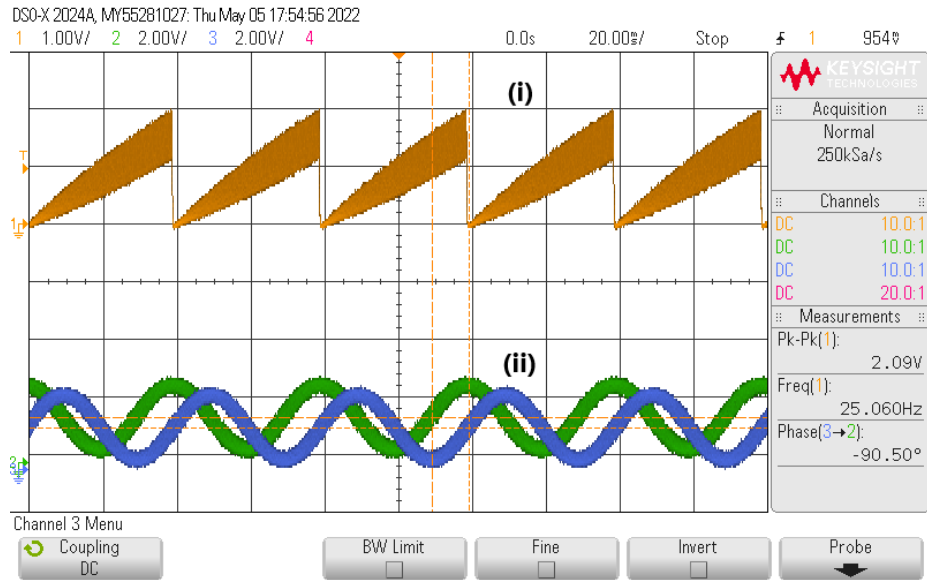


Figure 4.21: (i) θ corresponding to a 25 Hz modulating wave generated in the DSP (ii) Signal and 90° phase shifted version of the signal obtained using filter in the DSP.

- The results are taken by connecting a 10A/10Ω rated rheostats (R Loads), connected in a star manner. Once the IM starts generating, the inverter phase voltage and the machine current must be in quadrature (90° phase-shifted) with each other. This ensures that the VSI supplies all the reactive power needed for the excitation of IG. In

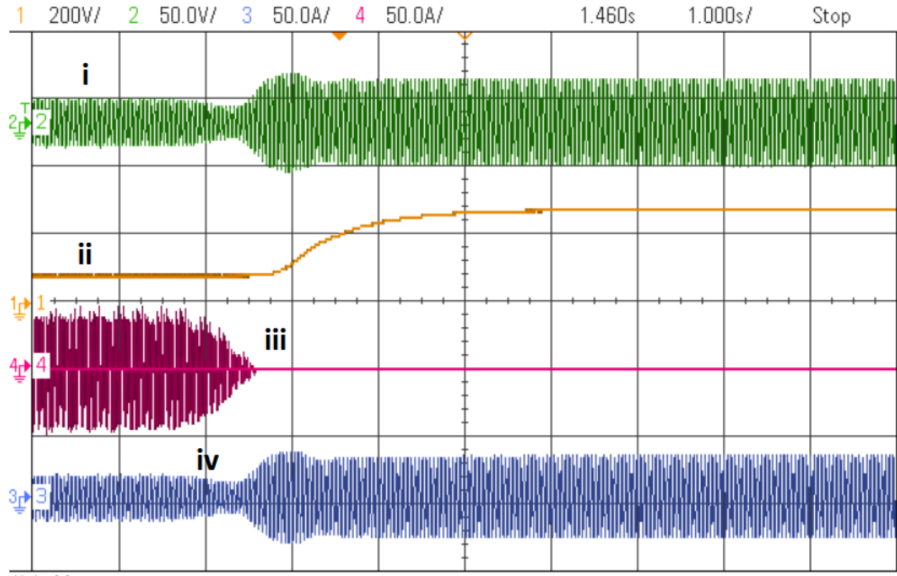


Figure 4.22: Waveform capturing the transition from motoring to generating mode [X axis: 1s/div] (i) Load Voltage [Y axis: 50V/div], (ii) Capacitor DC Link Voltage [Y axis: 200V/div], (iii) Rectifier (DBR) current [Y axis: 50A/div], (iv) Stator Phase Current [Y axis: 50A/div].

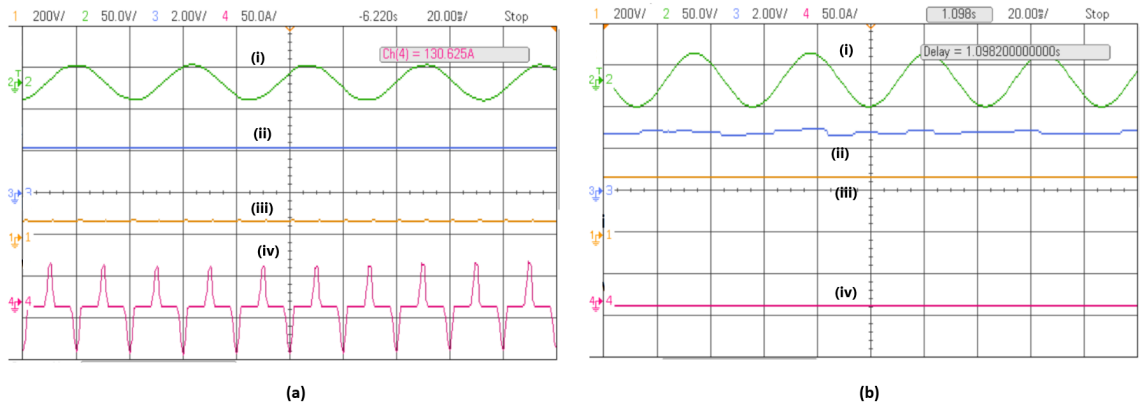


Figure 4.23: (a) IM in motoring mode and (b) IM in generating mode [X axis: 20ms/div] [X axis: 1s/div] (i) Load Voltage [Y axis: 50V/div], (ii) Capacitor DC Link Voltage [Y axis: 200V/div], (iii) Rectifier (DBR) current [Y axis: 50A/div], (iv) Stator Phase Current [Y axis: 50A/div].

Fig. 4.24, an approximate 90° phase shift between machine current and inverter phase voltage is seen, which concludes that our VSI is successfully able to deliver all the required reactive power.

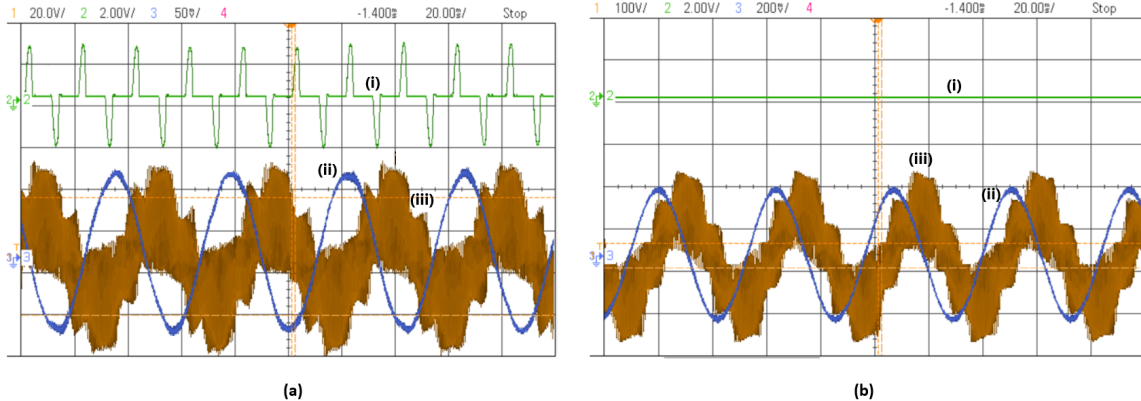


Figure 4.24: (a) IM in motoring mode and (b) IM in generating mode [X axis: 20ms/div] [X axis: 20ms/div] (i) Rectifier (DBR) current [Y axis: 2A/div], (ii) Machine Currents [200mA/div], (iii) Inverter Phase Voltage [Y axis: 100V/div].

4.4 Conclusions

In this chapter, various hardware modules used for experimental purposes are discussed. The experimental results of sine-triangle PWM, and reference frame transformations are presented. Then the results capturing the transition of IM from motoring to generating mode for a grid-connected system are discussed. In the later sections, the results capturing the series reactive power compensation of the IG using a capacitor fed VSI are presented. The experimental setups for implementing the whole control system for grid-connected and grid plus load connected systems are being developed, and the results will be updated here soon.

Chapter 5

Conclusions and Future Works

5.1 Results and Discussion

In this report, a reactive power compensation scheme for **grid-connected IG system** using series STATCOM has been discussed. This idea has been extended to come up with a reactive power compensation scheme for **grid and load connected IG system** using series STATCOM . The results for both systems are discussed in detail. The techniques developed mainly focus on maintaining a constant DC link voltage, UPF near the grid, and reactive power transfer between VSI and the IG. The results for both grid-connected and grid and load connected IG systems are presented along with their operation principles, phasor diagrams, and control schemes. A DC link voltage of 500V was given as a reference for the grid-connected case, and 300V was provided as a reference for the grid and load connected case. The DC link voltage stabilized at the desired reference value for both systems. The machine current and inverter pole voltage was observed to be in quadrature for both systems, suggesting that no active power transfer occurs between VSI and the IG. For the grid and load connected case, linear and non-linear load scenarios were simulated, and all the requirements were met for both balanced and unbalanced cases.

5.2 Future Works

Following is a brief list of tasks that can be completed in the future :

- Hardware implementation of the reactive power compensation scheme for grid and load connected IG system using series STATCOM is still pending . Exhaustive experimentation of the proposed system and its validation are to be done.
- With our proposed system, UPF near grid was achieved for non-linear DBR loads. But distortions were observed in the grid current waveform as seen in Fig. 3.13. Hence, coming up with better control schemes for non-linear loads that maintain UPF and overcome the distortion in grid current is still something left to be explored.
- Implementation of the same system in natural (abc) reference frame. In such a system, all the three phases work independently, and hence a better performance can be achieved when unbalanced load scenarios arise.
- Modelling and control of proposed system using *instantaneous pq theory*. Using the pq theory model, controllers and systems with better harmonic compensation can be designed. The conventional theory and controllers assume everything to be sinusoidal, and the distortions are neglected, but using pq theory, distortions is also accounted for.

Bibliography

- [1] R. Bansal, T. Bhatti, and D. Kothari, “Bibliography on the application of induction generators in nonconventional energy systems,” *IEEE Transactions on Energy Conversion*, vol. 18, no. 3, pp. 433–439, 2003.
- [2] R. Bansal, “Three-phase self-excited induction generators: an overview,” *IEEE Transactions on Energy Conversion*, vol. 20, no. 2, pp. 292–299, 2005.
- [3] S. Hazra, “Self-excitation and control of an induction generator in a stand-alone wind energy conversion system,” *IET Renewable Power Generation*, vol. 4, pp. 383–393(10), July 2010. [Online]. Available: <https://digital-library.theiet.org/content/journals/10.1049/iet-rpg.2008.0102>
- [4] V. Yaramasu, B. Wu, P. C. Sen, S. Kouro, and M. Narimani, “High-power wind energy conversion systems: State-of-the-art and emerging technologies,” *Proceedings of the IEEE*, vol. 103, no. 5, pp. 740–788, 2015.
- [5] W. Na, E. Muljadi, B. Leighty, and J. Kim, “Active power and flux control of a self-excited induction generator for a variable-speed wind turbine generation,” in *2017 Ninth Annual IEEE Green Technologies Conference (GreenTech)*, 2017, pp. 177–181.
- [6] N. Garcia and E. Acha, “On the efficient calculation of the periodic steady-state response of grid-connected wind parks—part i,” *IEEE Transactions on Sustainable Energy*, vol. 8, no. 2, pp. 458–467, 2017.

- [7] E. Suarez and G. Bortolotto, “Voltage-frequency control of a self-excited induction generator,” *IEEE Transactions on Energy Conversion*, vol. 14, no. 3, pp. 394–401, 1999.
- [8] B. Singh, S. Murthy, and S. Gupta, “Statcom-based voltage regulator for self-excited induction generator feeding nonlinear loads,” *IEEE Transactions on Industrial Electronics*, vol. 53, no. 5, pp. 1437–1452, 2006.
- [9] E. Muljadi and T. Lipo, “Series compensated pwm inverter with battery supply applied to an isolated induction generator,” *IEEE Transactions on Industry Applications*, vol. 30, no. 4, pp. 1073–1082, 1994.
- [10] D. Pan, Y. Wang, and T. A. Lipo, “A series regulated open-winding pm generator based constant voltage, variable frequency ac distribution system,” in *2013 IEEE ECCE Asia Downunder*, 2013, pp. 214–220.
- [11] Y. Jia and K. Rajashekara, “An induction generator-based ac/dc hybrid electric power generation system for more electric aircraft,” *IEEE Transactions on Industry Applications*, vol. 53, no. 3, pp. 2485–2494, 2017.
- [12] Y. Jia, U. R. Prasanna, and K. Rajashekara, “An open-end winding induction generation system for frequency insensitive ac loads in more electric aircraft,” in *IECON 2014 - 40th Annual Conference of the IEEE Industrial Electronics Society*, 2014, pp. 410–416.
- [13] G. Athira, R. Sudharshan Kaarthik, and P. Rajeevan, “An open end winding induction generator system for simultaneous supply of power to dc-link loads and frequency insensitive ac loads with voltage regulation,” in *2018 IEEE International Conference on Power Electronics, Drives and Energy Systems (PEDES)*, 2018, pp. 1–6.
- [14] C. M. Archana, P. Rajeevan, and S. Kaarthik, “A series compensated open-end winding induction generator system for dc loads and ac linear, non-linear and unbalanced loads,”

in *2018 8th IEEE India International Conference on Power Electronics (IICPE)*, 2018, pp. 1–6.

- [15] E. Volt, “Torque slip characteristics of induction motor by electrical volt.” [Online]. Available: <https://www.electricalvolt.com/2018/12/torque-slip-characteristics-of-induction-motor/>
- [16] S. Gadipudi, P. Rajeevan., and R. S. Kaarthik, “A grid connected open-end winding induction generator system with series compensation,” in *2020 IEEE International Conference on Power Electronics, Smart Grid and Renewable Energy (PESGRE2020)*, 2020, pp. 1–4.
- [17] J. Hu and Y. He, “Reinforced control and operation of dfig-based wind-power-generation system under unbalanced grid voltage conditions,” *IEEE Transactions on Energy Conversion*, vol. 24, no. 4, pp. 905–915, 2009.
- [18] A. Lantero, “Department of energy - how microgrids work.” [Online]. Available: <https://www.energy.gov/articles/how-microgrids-work>

Appendix A

Appendix A

A.1 Hardware Modules

A.1.1 3- ϕ Auto-transformer

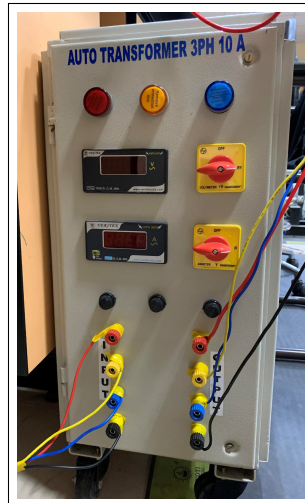


Figure A.1: 3- ϕ Auto-transformer in Laboratory.

- The 3- ϕ Auto-transformer takes the 3- ϕ RYB supply from the grid and generates a 3- ϕ RYB output that can be set to any value per our need. It is essentially a transformer that converts supply voltage to our desired voltage level. Note that the value mentioned on it is the rotary knob is the RMS value of the output voltage waveform.

A.1.2 Voltage Sensor Board

- The output voltage from the 3- ϕ auto-transformer may range from a low value to a very high value (up to 400V). Such high voltages must be sensed and properly scaled down before passing to further system blocks.
- The voltage sensor board has three such sensors. Each sensor works independently and can sense AC and DC voltages of up to 1000V. The VH1K0T01 voltage sensor IC scales down the voltage within [-5V,+5V].
- This module requires a DC supply of $\pm 15V$. It is equipped with a galvanic isolation between the high voltage primary and the secondary circuit (electronic circuit).

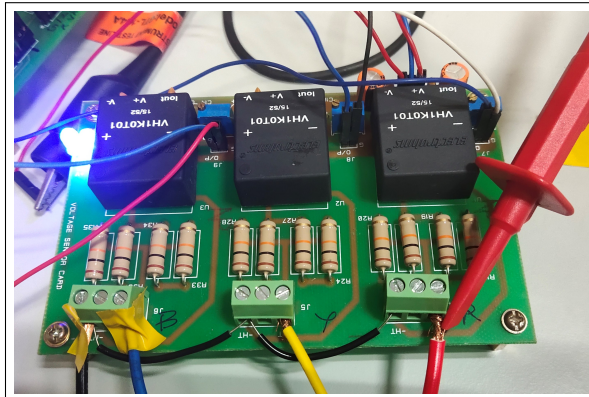


Figure A.2: 3-channel Voltage Sensor Module.

A.1.3 Level Shifter Board

- The voltage values sensed from the voltage sensors has to be further processed by the DSP board. This is enabled with the help of the ADC module on the TMS320F28069M board. However, the ADCs available on this board are unipolar, which means they can process only positive signals.
- The level shifter board takes the signals from the voltage sensor board and shifts them

up by adding an offset. This board essentially converts the bipolar signals into unipolar signals and enables interfacing with the ADC on the DSP board.

- This module requires a DC supply of 5V.



Figure A.3: Level Shifter Module.

- The ADC module on the DSP board is 12-bits (meaning a range of 4096 levels), and the expected signal input to this ADC is within [0,+3.3V].
- The output of Voltage Sensor and Level Shifter must be tuned so that the signal to ADC input is within the [0,+3.3V] range. This can be done by turning the potentiometers on the voltage sensor board.

A.1.4 TI TMS320F28069M DSP Board

- Hardware implementation of the control scheme requires a digital signal processor (DSP) that can perform floating-point operations at a fast rate. All the varying parameters, such as current or rotor speed, must be continuously sensed. They need to be processed in real-time to maintain the system's desired state.
- All the processing, reference frame transformations, control loop implementations, gate switching pulse generations, etc., are performed on the DSP board.

- Code Composer Studio (CCS) software is used to program the DSP module.

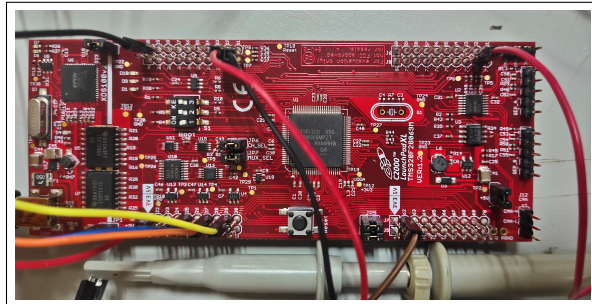


Figure A.4: TMS320F28069M DSP Module.

A.1.4.1 Specifications of the TMS320F28069M DSP Module

- Clock frequency of 90 MHz
- 8 ePWM modules for PWM generation
- 2 Enhanced Quadrature Encoder Pulse (eQEP) modules
- 12 bit A/D Converter module with two parallel converters (ADC)
- 54 GPIO (Input/Output) pins
- No independent DAC module is available. ePWM 7 and 8 module outputs can be configured to pass via an internal RC filter and give a DAC-like operation.

A.1.4.2 Modules of DSP

The main modules present on the DSP that are used for the implementation are as follows:

A.1.4.3 Enhanced Pulse Width Modulation (ePWM)

- This module sets the interrupts that are triggered to maintain the timing of code execution. This module also generates the switching PWM pulses to inverter gates.
- ePWM module uses the registers TBCTR (Timer Based Counter) and TBRPD (Timer Based Period) to generate the switching pulses, and these registers are user-configurable.

The ePWM modules are configured in the UP-DOWN mode. A symmetrical triangular waveform is used for the PWM signals generation, and this triangle has a peak value and time period equal to TBPRD.

A.1.4.4 Enhanced Quadrature Encoder Pulse (eQEP)

- This module is used to read the speed output by a rotary encoder. An optical rotary encoder gives two streams of output pulses: the relative phase difference gives the direction of rotation, and the frequency of pulses gives the speed of rotation.
- Other alternatives to measure the speed of the motor is to use (a) Tachometer or (b) to measure the time period of the impulse sequence signals obtained from the IG's rotary encoder.

A.1.4.5 Analog to Digital Converter (ADC)

- When implementing controllers that require voltage/currents sensed in the feedback, the outputs of the voltage sensors and Hall-Effect-based current sensors should be digitized before applying as input to the DSP. For this purpose, the DSP board has a 12-bit A/D Converter module with two parallel converters (ADC).

A.1.5 3- ϕ Inverter

- The 3- ϕ inverter module used in the project is as shown in Fig. A.5. It consists of SEMIKRON SKM100GB12T4 IGBT modules have a voltage rating of 1200V and a current rating of 100A. It has a rated switching frequency of 20KHz.
- This module also contains a 3- ϕ diode bridge rectifier, four Hall-Effect-based current sensors (LA55-P), and one LV20-P voltage sensor. The VSI has four legs, out of which any three can be used for the experiment purpose.

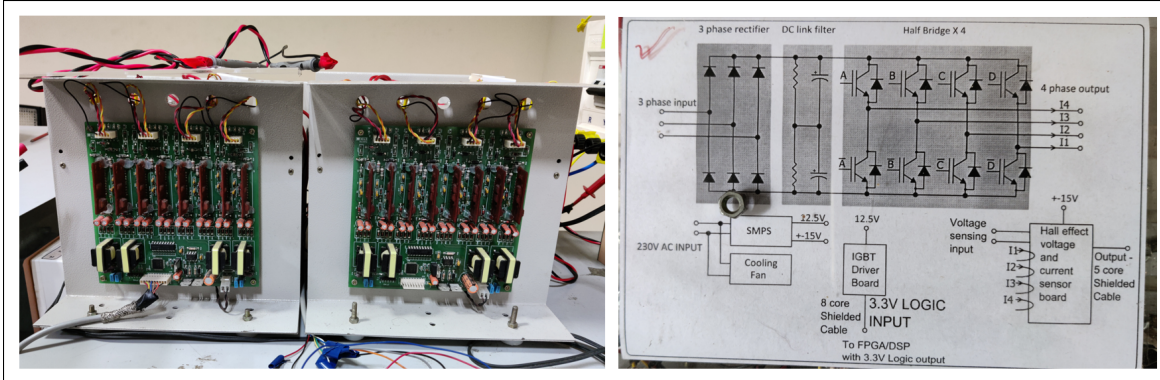


Figure A.5: 3- ϕ Inverter Module with DBR and Hall-Effect Current/Voltage Sensors.

A.1.6 Hall Effect Current Sensors

- Hall effect current transducer LA55-P is used to sense the three-phase currents and give as feedback to the DSP (Fig. A.6).

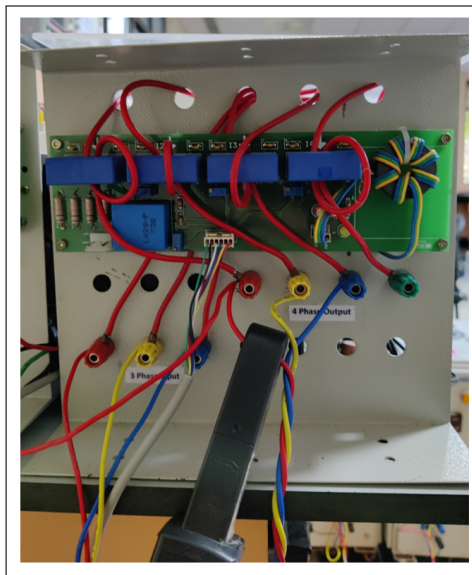


Figure A.6: Hall-Effect based Current Sensors.

- It has a wide range of measurements ranging from a few mA to 50A. The number of turns around the sensor is increased to obtain higher sensitivity. The sensors are calibrated separately, and individual sensor gains are found before the experiment.

A.1.7 3- ϕ Induction Generator with open-end stator windings

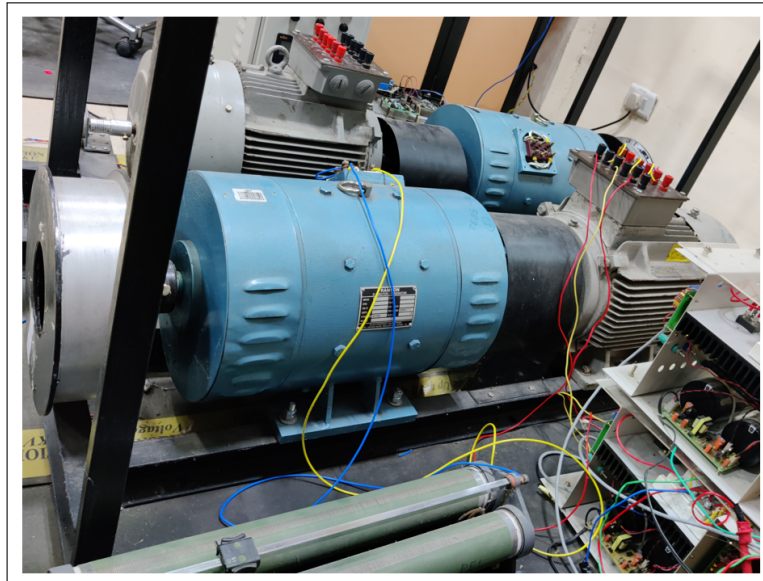


Figure A.7: 3- ϕ Induction Machine with DC Motor.

- SIEMENS 3- ϕ induction motor with a RAMSON DC motor/generator coupled to its shaft is used for experimental purposes in the laboratory (Fig. A.7). The DC motor is coupled to the shaft of the IM and is used as a prime mover to make the IM operate as a generator. The specification of the induction machine and DC motor are as follows:

Table A.1: Specifications of Induction Machine and DC Motor

S.No	Induction Machine Specifications	DC Motor Specifications
1	Rated Voltage: $415V \pm 10\%$	Rated Voltage: 220V
2	Rated Current: 21A	Rated Current: 50A
3	Power Rating: 11kW	Power Rating: 11kW
4	Rated Speed: 1440 rpm	Rated Speed: 1500 rpm
5	Rated Frequency: 50Hz	Type: DC Shunt Motor

